(2)

DOE/ET/23008-T1

EMERGING MATERIALS FOR SOLAR CELL APPLICATIONS—ELECTRODEPOSITED CdTe

Final Report, February 14, 1979—February 14, 1980

By
Robert L. Rod
Rointan Bunshah
Oscar Stafsudd
Bulent M. Basol
Prem Nath

May 15, 1980

Work Performed Under Contract No. AC04-79ET23008

Monosolar, Inc.
Santa Monica, California

U.S. Department of Energy

Solar Energy

DISCLAIMER

DISCLAIMER

Available from the National Technical Information Service, U. S. Department of Commerce, Springfield, Virginia 22161.

Price: Paper Copy $8.00
Microfiche $3.50

DOE/ET/23008-T1
Distribution Category UC-63e

EMERGING MATERIALS FOR SOLAR CELL APPLICATIONS – ELECTRODEPOSITED CdTe

FINAL REPORT
FOR PERIOD FEBRUARY 14, 1979 – FEBRUARY 14, 1980

ROBERT L. ROD
ROINTAN BUNSHAH
OSCAR STAFSUDD
BULENT M. BASOL
PREM NATH

MAY 15, 1980

MONOSOLAR, Inc.

a subsidiary of

Monogram Industries, Inc.

Suite 600
100 Wilshire Blvd.
Santa Monica, CA 90401

PREPARED FOR THE
U.S. DEPARTMENT OF ENERGY
SOLAR ENERGY
UNDER CONTRACT DE-AC04-79ET23008

Program Participants

The principal investigator for Monosolar, Inc. was Robert L. Rod. Other Monosolar program members and participants in this report's preparation were Eric Tseng, Walter Penick, Ricardo Campos, and Zvi Shkedi.

Co-principal investigators at the University of California - Los Angeles were Professors Oscar Stafsudd and Rointan Bunshah. They were assisted by Bulent Basol and Prem Nath.

ABSTRACT

Thin film gold/polycrystalline cadmium telluride Schottky solar cells made by electrodepositing the semiconductor on an ITO-coated glass substrate serving also as an ohmic contact demonstrated an internal efficiency of 4% over 2 mm^2 areas. This program is a continuation of earlier ERDA- and DOE-funded efforts wherein the contractor reduced to practice the underlying theory of cathodically plating compound semiconductors.

During the year being reported upon, Monosolar devoted major attention to refining the electroplating process and determining the parameters governing CdTe film stoichiometry, grain size, substrate adhesion, and quality. UCLA acting as a Monosolar sub-contractor characterized both the CdTe films themselves and solar cells made from them. Techniques were developed for making measurements on films often less than 1 micron in thickness. These also are applicable to other researchers in the field.

The highest values achieved for efficiency parameters, not necessarily all in the same cell, were V_{oc} = 0.5 V, J_{sc} = 11 mA/cm^2, and fill factor = 0.55 before corrections in the absence of anti-reflection coatings. Typical resistivities for n-CdTe films were 10^5 Ω-cm. Lifetimes of about 10^{-10} sec were measured. Absorption coefficient of these films is in the order of 10^4 for $\lambda < 0.7$ μm. Measured energy gap for these CdTe films is 1.55 eV, slightly higher than the 1.45 eV value for single crystal CdTe. The activation energy of the dominating trap level is 0.55 eV. Trap density is in the order of $10^{16}/cm^3$.

Schottky diodes were of excellent quality and pinhole-free. The measured barrier height varied between 0.75 and 0.85 eV. Rectification ratios of 10^4 were obtained reproducibly. Films measure about 1 inch square. Indications are that larger and more efficient low cost solar devices can readily be obtained soon using the techniques developed in this program.

TABLE OF CONTENTS

TABLE OF CONTENTS (Continued)

LIST OF FIGURES

LIST OF FIGURES (Continued)

LIST OF TABLES

I. OBJECTIVES OF THE PROJECT

This program has as its general long-range objective the development of 10% efficient thin film polycrystalline solar cells by 1980 having the potential for manufacture at $0.30/peak watt by 1986. It had its onset in 1973 when Monosolar's parent company, Monogram Industries, Inc., undertook initial development of techniques for electrodepositing thin polycrystalline films of II-VI compound semiconductor materials. Later, cost-sharing support of this work was obtained first from ERDA and then DOE. The basic theory underlying this method of film preparation was explored by Monosolar's subcontractor, the University of Southern California. The findings were presented in both governmental reports and the literature[1,2,3].

The specific objectives of the present effort were several fold. One required fabrication by electrodeposition of 2.5 x 2.5 cm^2 ITO/CdTe solar cells free from pinholes. Cells were first to be characterized for efficiency. Then the fill factor, V_{oc}, and J_{sc} were to be examined as functions of such parameters as plating temperature (grain size) and plating current (deposition time), layer thickness, pinhole densities (if any), stoichiometry (Te concentration greatly affecting V_{oc}), doping levels and others. Structural and compositional parameters of the various layers were then to be evaluated using available techniques known to be applicable to such thin film devices.

All of these objectives were satisfied during the term of the program with the exception of work relating stoichiometry of the films to device performance. That work is now completed at this writing after the contractor purchased an atomic absorption spectrophotometer needed to make the

required analyses of both electrolytes and film samples dissolved in acid. A continuation of the program under SERI sponsorship that began on February 16, 1980 will result in fabrication of 4%-efficient cells over an area of 1 cm^2 by the fall of 1980 and more efficient ones possibly by late winter.

II. SUMMARY OF THE PROGRESS ACHIEVED

Work during the year being reported upon was divided into two parts. Monosolar assumed responsibility for producing CdTe films in its facilities, while UCLA as a subcontractor was required to characterize the films and devices made from them. Heretofore no methods had been found to make even such simple measurements as finding the bulk resistivity of thin semiconductive films a micron or less in thickness which were deposited over highly conductive substrates. Nor could one determine n-ness or p-ness of such films by thermoelectric means with any degree of accuracy. Similarly, Hall effect measurements were complicated not only by the geometry but also the fact that the films being produced showed resistivities in the order of 10^5 Ω-cm or higher.

These measurement difficulties reflected back as problems to those charged with the electroplating. Changes in plating parameters, such as electrolyte pH, tellurium ion concentration, deposition and rest potentials, and plating current initially could not be correlated with device performance.

Control over the whole process first began to be achieved when A.A. spectrophotometer determinations of the Cd and Te levels in the electrolytes as a function of time were undertaken at an outside laboratory. It was found during the electrolyte purification process using a dummy cathode that the Te ion concentration varied widely for several days. Cells produced during that time were not reproducible one after the next. Knowing this, it then became possible to develop a procedure for maintaining the Te ion concentration at desired levels. Later on, the necessary equipment to do this was purchased by Monosolar for in-house use. To facilitate measurement work, the Monosolar/UCLA team devised an epoxy technique to strip films from their ITO or nickel substrates for study of their semiconductor properties.

One end result of this program was the routine production of two reproducible classes of Schottky solar cells. One of the classes used evaporated Au on top of CdTe films electroplated in the original $CdSO_4$-based electrolyte at pH values around 2 and at a bath temperature of 90°C. Cells made this way showed the highest V_{oc} but lower values of J_{sc} than those achieved using a second and newer bromide-based aqueous electrolyte also at pH of 2 and 90°C. The latter electrolyte yielded devices having J_{sc} values twice those of cells made in the sulfate bath and double the solar efficiency.

III. ELECTRODEPOSITION OF CADMIUM TELLURIDE

1. Plating Techniques

Cathodic deposition of CdTe most often was carried out in an aqueous electrolyte solution containing cadmium sulfate and $HTeO_2^+$ ions (5 - 20 ppm) at a pH around 2 and at a temperature around 95°C. Some work also was done using a bromide-based electrolyte under similar conditions. Ni- or ITO-coated glass substrates served as cathodes. The anode was either inert graphite or tellurium metal. They were used separately or together depending on the desired Te ion concentration. The deposition reactions are:

$$HTeO_2^+ + 3H^+ + 4e^- \rightarrow Te + 2H_2O \qquad E^o = +0.31 \text{ V vs. SCE}$$

$$Cd^{2+} + 2e^- \rightarrow Cd \qquad E^o = -0.64 \text{ V vs. SCE}$$

$$Cd + Te \rightarrow CdTe \qquad 4G^o = -25.5 \text{ Kcal/mole}$$

During the plating process, the reaction between Cd and Te shifts the Cd deposition potential less negative. Thus, Cd and Te can be co-deposited at a cathode potential between -0.10 V and -0.64 V vs. SCE depending on the desired stoichiometry of the deposit. More negative potentials yield Cd-rich deposits while less negative potentials yield Te-rich deposits[2,3].

At room temperature the deposits are either very fine grained or amorphous. At a plating temperature around 95°C all deposits are polycrystalline with a grain size typically 0.1 to 1.0 μm. The current density mainly depends on $HTeO_2^+$ concentration, pH, the stir rate and deposition potential selected. Columnar growth, pinhole-free CdTe films have been

obtained at a plating current density between 0.2 - 0.5 mA/cm^2. Excessively low current tends to create discontinuous grains; too high a current creates pinholes.

Fig. 1 illustrates the plating system. Film deposition takes place in a 2000 ml beaker into which the substrates are lowered by an electrical contact clamp. Electrolyte is agitated by means of a magnetic stirrer built into the electrical hot plate heating the bath to 95°C.

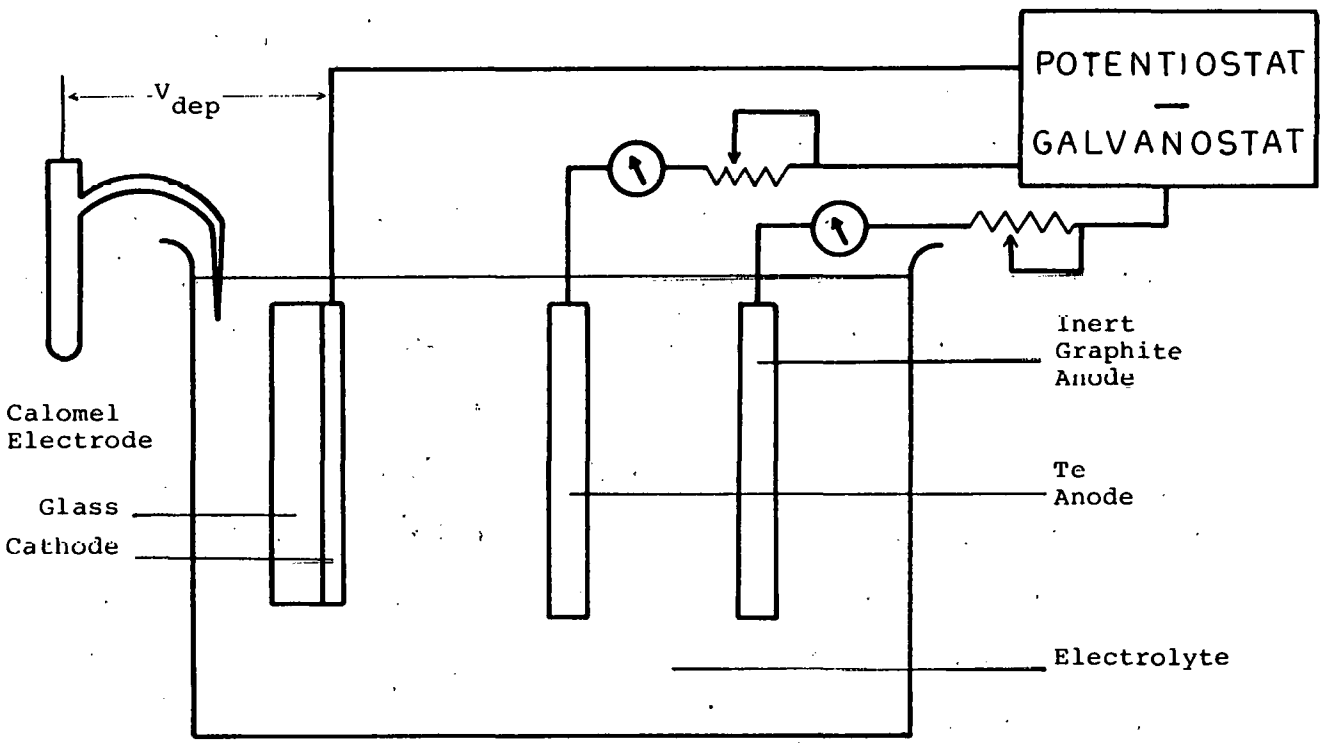

Figure 1. Cathodic Plating System for CdTe

During this one year period, 800 films were made. 600 films were deposited on PPG's ITO-coated glass, and 200 films were deposited on Ni-coated glass. Co-deposited n- and p-type dopants were also studied. (Table 1)

TABLE 1

Breakdown of Film Production by Types

dopants/ # of films/ substrates	undoped	In	As
ITO on glass	250	200	150
Ni on glass	70	50	80

2. Electrolyte Purification

Electrolytes must be purified to semiconductor quality levels before actual electrodeposition of CdTe commences. This is accomplished by well-known electrochemical techniques. During a 24 hour purification period, those impurities having an electrochemical potential more positive than Cd are plated out on a dummy cathode of ITO or Pt to levels below 0.1 ppm. Impurities having electrochemical potentials more negative than the Cd potential are of no concern unless present in substantial amounts. Table 2 shows the major impurities which are present in commercial reagent-grade $CdSO_4$ before and after purification. Measurement was done by A.A. spectrophotometry. $CdSO_4$ solution was 0.5 M.

TABLE 2

Electrolyte Purification Effectivity

impurities/ conc. in ppm/ electrolytes	Cu	Fe	Pb	Ni	Zn
before purification	2.0	0.3	1.0	0.07	1.1
after purification	0.005	0.1	0.1	<0.01	1.0

Cu, Fe, Pb and Ni which have more positive potentials than Cd are plated out. Zn, which has a more negative potential than Cd, stays at the same level.

After purification, the $HTeO_2^+$ ion then is introduced into the electrolyte by using a Te anode and adjusting the plating current to achieve the desired Te ion concentration. Good CdTe films are obtained 16 hours following initial Te introduction.

3. Impurities

Foreign impurities finding their way into initially purified electrolytes during earlier plating processes were first identified and then eliminated. Table 3 shows the major impurity levels in fresh and used $CdSO_4$ electrolytes (after one month of plating) and in dissolved CdTe films.

TABLE 3

Electrolyte Impurity Buildup

impurity/ conc. in ppm/ electrolytes on film	Cr	Ni	Al	Ca	Mg	Na	Cu	Zn
Fresh $CdSO_4$ electrolyte	0.09	0.07	<0.01	0.2	0.08	0.2	2.0	1.1
Used electrolyte	0.68	1.8	4.6	5.0	1.2	15	<0.001	1.0
Wt of impurities in CdTe film/ Wt of CdTe film	0.0029	0.19	$<10^{-9}$	$<10^{-9}$	$<10^{-9}$	0.0014	$<10^{-10}$	$<10^{-10}$

The major source of Al, Ca, Mg and Na impurities was identified as a contaminated fiberglass filter element through which the electrolyte was circulated. Removal of the filter from the system cured the problem. Cr contamination resulted from dragout of the acid-dichromate solution used to clean the substrates. Careful rinsing procedures removed the Cr contamination. Ni contamination resulted from etching of those substrates by the electrolyte. This problem was solved only by discontinuing the use of Ni substrates for n-CdTe devices in favor of ITO.

4. Dopant Co-deposition

Different levels of the In^{3+} ion were added into electrolytes to study co-deposition of In into CdTe to form n-type films. Table 4 shows the relationship between In concentration in the electrolytes and that in dissolved doped CdTe films (films deposited on Ni substrates). Measurement was done by A.A. spectrophotometry.

TABLE 4

Dopant Co-Deposition

conc. Sample #	[In] in plating bath (ppm)	[In] in dissolved CdTe (ppm)	[Cd] in dissolved CdTe (ppm)	[Te] in dissolved CdTe (ppm)	In/CdTe wt ratio	atoms of In/ cm^3 CdTe	Av. plating QRP (mV)*
NS-1	5	0.03	510	600	2.7×10^{-5}	8.4×10^{17}	575
NS-2	5	0.03	520	450	3.1×10^{-5}	9.5×10^{17}	580
NS-3	5	0.03	430	600	2.9×10^{-5}	8.9×10^{17}	570
NS-31	60	0.25	270	260	4.7×10^{-4}	1.4×10^{19}	545
NS-32	60	0.19	220	170	4.9×10^{-4}	1.5×10^{19}	500
NS-33	60	0.12	200	180	3.2×10^{-4}	9.7×10^{18}	495
NS-37	190	0.55	300	290	9.3×10^{-4}	2.8×10^{19}	540
NS-38	190	0.32	250	160	7.8×10^{-4}	2.4×10^{19}	510
NS-39	190	0.34	270	260	6.4×10^{-5}	2.0×10^{19}	460
NS-44	1900	1.08	270	260	2.0×10^{-3}	6.2×10^{19}	555
NS-45	1900	0.40	130	50	2.3×10^{-3}	7.0×10^{19}	530

*QRP - Quasi-rest potential

A plot of In concentration in plating solution against atoms of In/cm^3 CdTe is shown in Fig. 2.

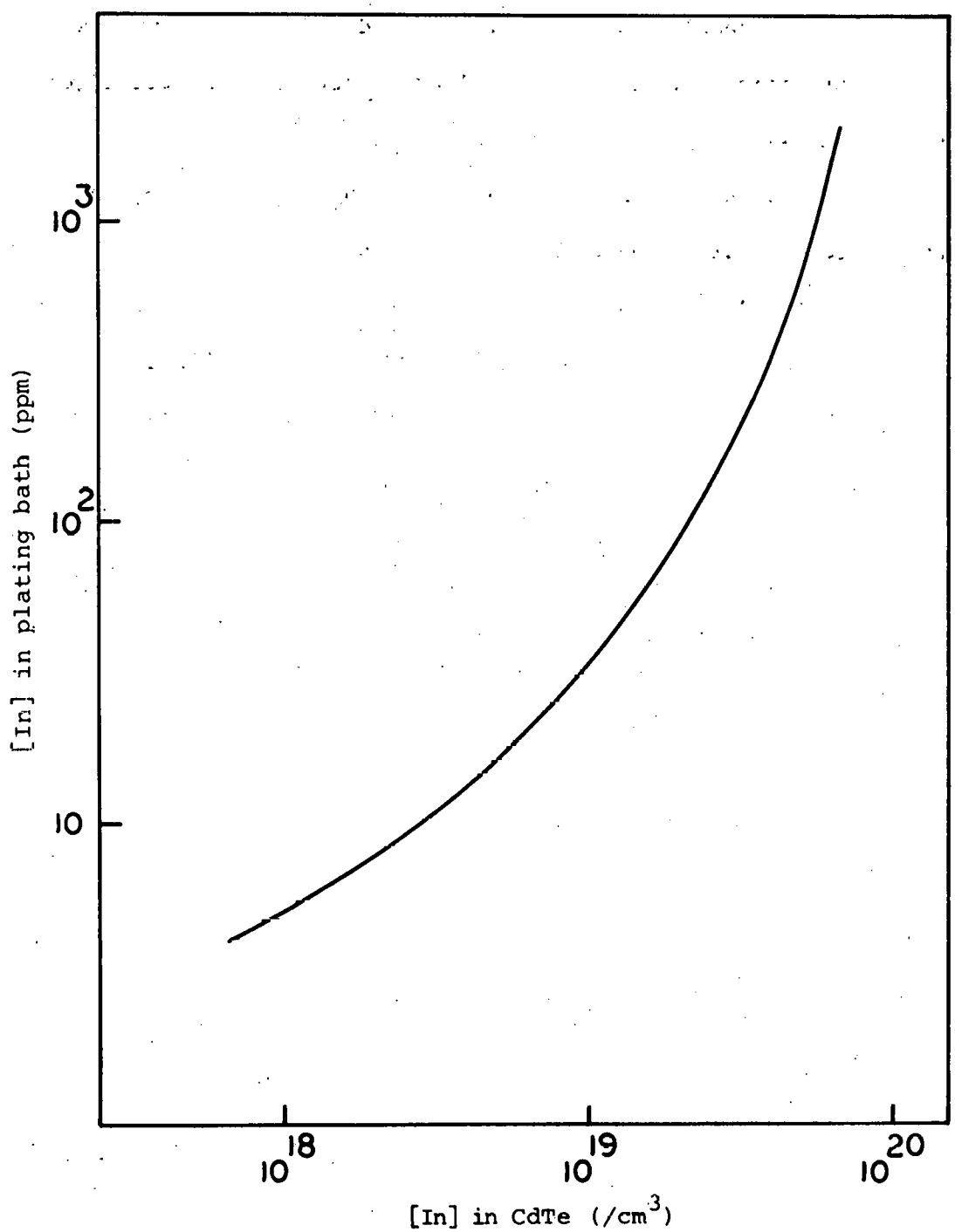

Figure 2. [In] in the Plating Solution vs. in CdTe Films

The lowest measured value for resistivity of n-CdTe:In films was about 10^5 Ω-cm and was more a function of the selected deposition potential than the level of indium in the CdTe film. Apparently some additional step is required to activate the indium in the event that a lower value of resistivity is needed. Thermoelectric probe techniques were used in classifying the material as n-type.

Compared to the results achieved doping CdTe with In, the attempts to co-deposit an acceptor into CdTe to form p-type material were unsuccessful. For As-doped CdTe, chemical analyses showed that the As level in the films, if any, was lower than the detecting limit (0.01 ppm in solution). Thermoelectric probing never gave a sharp indication of p-type material with As or Sb or Au used as acceptors.

IV. FILM CHARACTERIZATIONS

1. Materials Properties of Electrodeposited CdTe Films

Materials properties of the electrodeposited CdTe films are strongly dependent on the deposition temperature. Room temperature deposits are very fine grain or amorphous. Increased deposition temperature improves the crystallinity. The films deposited at 90-95°C, the highest possible temperature not exceeding the boiling point of the aqueous solution, are polycrystalline with grain sizes in the order of 0.2-0.5 μm. There are no porosity or pinhole problems for films thicker than about 0.2 μm. Density measurements on films made late in this program give a number close to that of crystalline CdTe (6 gm/cm^3). The films' polycrystalline nature is demonstrated by X-ray diffraction as well as by TEM micrographs taken on very thin films that are stripped from their substrates. Figure 3 shows a typical X-ray diffraction pattern of a CdTe film on glass/evaporated Ni substrate. The intensity of the <111> peak suggests a <111> preferred orientation for the films. This is in agreement with previous reports.[1] The strong Ni peak observed is due to the substrate. Figure 4 is the SEM picture of a ~1 μm thick CdTe film. The surface topology is typical, and it does not allow positive identification of grain size and/or structure. However, the TEM picture of Figure 5 does allow the determination of a thin (~0.2 μm) film. This film shows a characteristic grain size of about 0.2 μm. Thicker films will almost certainly have grains of 0.2 μm as a minimum.

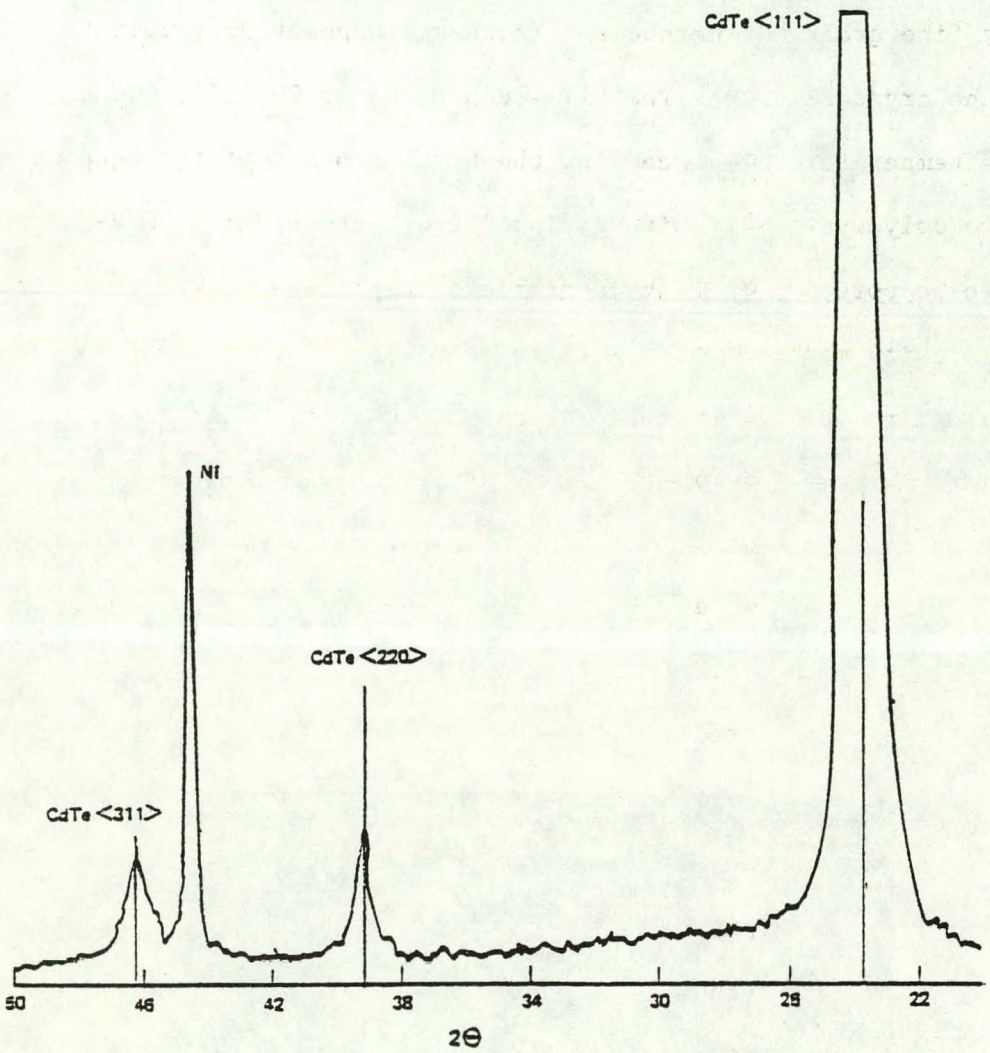

Figure 3. X-ray Diffraction Pattern of a CdTe Film

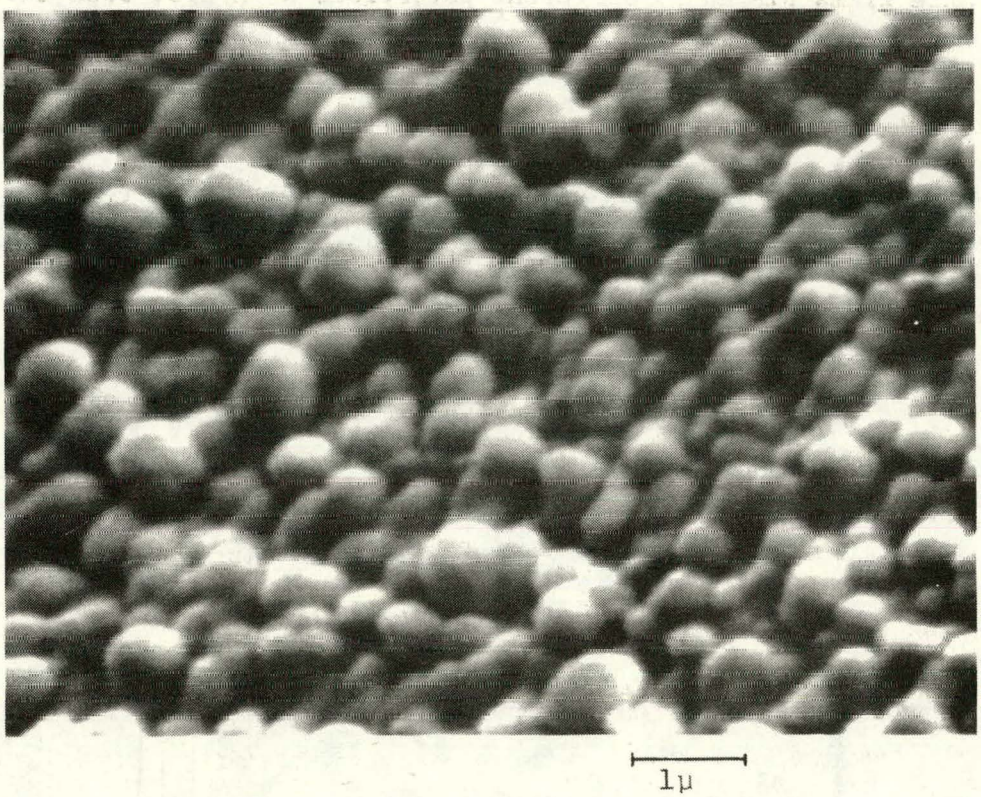

Figure 4(a). SEM Picture of the CdTe Film Surface

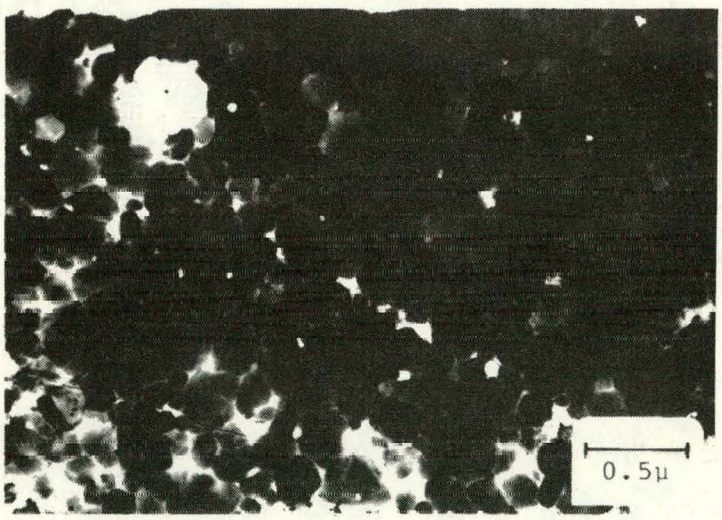

Figure 4(b). TEM Picture of a Thin CdTe Film Peeled Off Ni Substrate

CdTe films plated at different potentials have also been investigated by scanning electron microscopy and electron microprobe analysis. The studies showed the presence of particles/crystallites on the smooth surface of the CdTe film that varied in density and size with plating potential. Particle size decreases with increasing plating potential as is summarized in Table 5.

TABLE 5

Surface Particulate Size as a Function of Plating Potential

Plating Potential re SCE	Average Particle Size in Microns
-300 mV	---
-400 mV	5.7
-550 mV	5.0
-600 mV	1.0

In order to characterize these heretofore unknown particles, energy dispersive x-ray analysis (EDAX) was carried out on a SEM. The studies indicated that the particles are made up of Cd and Te as shown from the EDAX spectra in Fig. 5(a). The film surface and the particles showed identical EDAX spectra indicating identical composition for the particles and the film.

In order to evaluate the changes in CdTe film stoichiometry as a function of plating potential, electron microprobe analysis was performed on CdTe films deposited at different plating potentials. The studies show that the Cd/Te ratio in the films can be changed by as much as 7-8% by

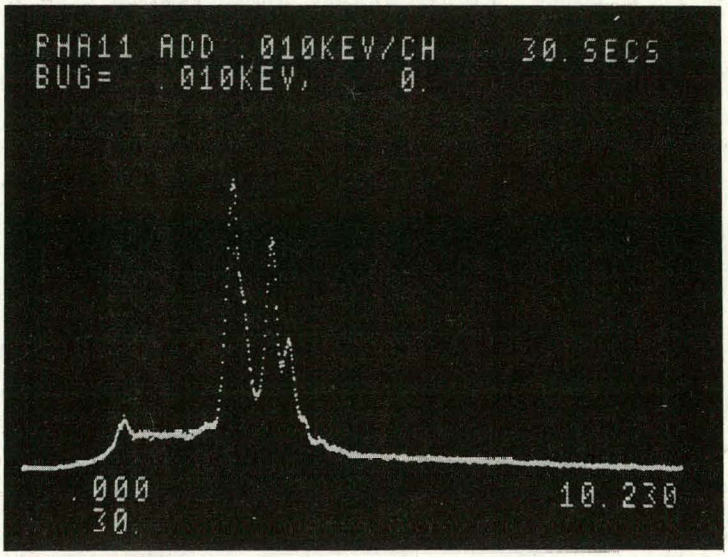

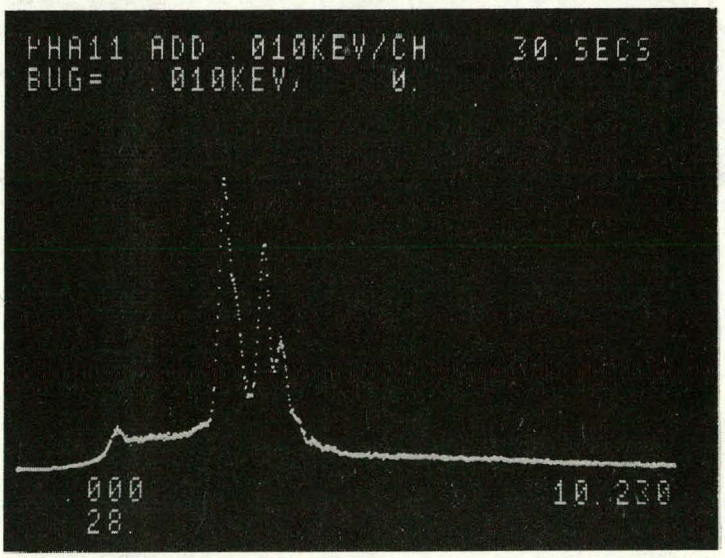

Figure 5(a). EDAX Analysis of Surface Particulates

varying the plating potential from -300 to -700 mV. The non-normalized Cd/Te ratio as a function of plating potential is shown in Fig. 5(b). It may be pointed out that the large error bar in specimen plated at -700 mV is due to the small thickness of this film as compared to the others.

Electrodeposited CdTe films have also been etched in several etchants in order to more clearly reveal the crystalline structure of the films. Etchant E-Ag-2 was the most successful, and a few large grains of CdTe have been identified in an optical microscope. The triangular shape which is typical of a <111> oriented crystal is observed. This is in agreement with the x-ray diffraction data.

2. Electrical and Optical Evaluation of the Films

Problems associated with the electrical evaluation of early films of electrodeposited CdTe were:

i) The I-V characteristics of early devices were dominated by a large shunt conductance. Therefore, these measurements did not yield data needed to properly characterize the films.

ii) Since the electrodeposited films are deposited on highly conductive substrates, the standard tools of semiconductor research, such as Hall effect, photoconductivity, etc. requiring measurement in the plane of the films, were inapplicable.

Both of these major problems have been overcome in the present research by:

i) Successfully preparing good quality Schottky barrier devices on pinhole-free electrodeposited CdTe layers which have rectification ratios as high as 10^4 at 1 volt applied bias.

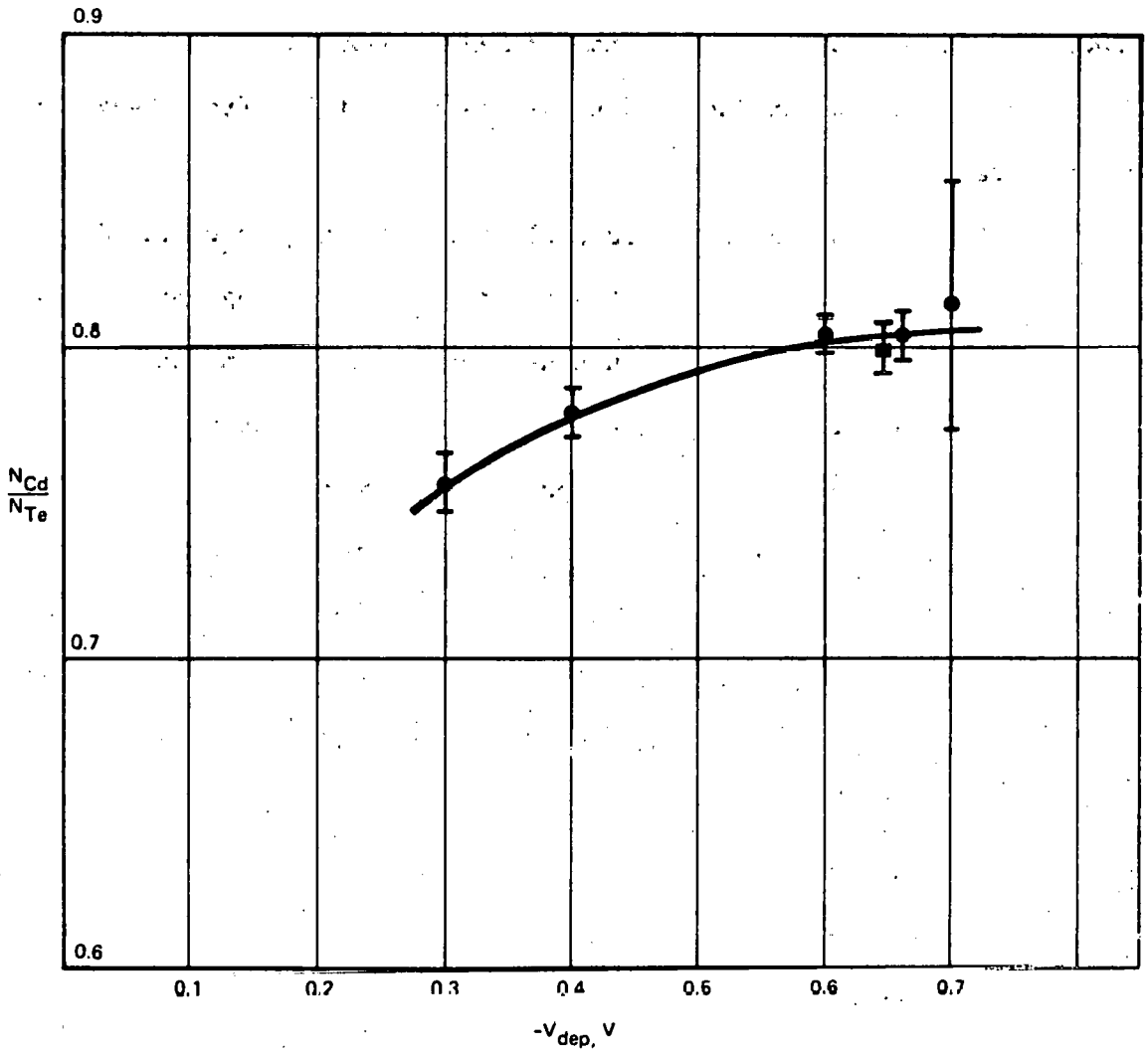

Figure 5(b). Microprobe Analysis of CdTe Film as a Function of Plating Potential

ii) Devising a method to transfer the films from their conductive substrates onto insulating substrates whereupon their characteristics could be determined.

While i) allowed the use of I-V and C-V measurements ii) made the resistivity and photoconductivity measurements possible.

Two methods were devised to separate the films from their conductive substrates:

i) Insulating epoxy was applied to the surface of the film. Both the glass substrate and its ITO coating were etched away with HF in an ultrasonic cleaner leaving behind the CdTe film. One problem with this technique was that if the etching of the glass was not uniform and some parts of the film were exposed to HF more than others, one got Te rich islands on the film which reduced the useful area for measurements.

ii) A simpler and more reproducible technique was mechanically stripping CdTe films from their ITO-coated glass or nickel substrates. Again an insulating epoxy applied to the CdTe was used. This method provided large area films with smooth, crack-free surfaces.

Best contacts to these films were obtained by Indalloy Solder #8 applied after a light film etch with 0.5% Bromine-Methanol solution that was aged for over three days. Linearity of the contacts can be observed from Fig. 6 which shows the I-V data obtained from two samples of relatively low resistivity ($\sim 10^5$ Ω-cm) CdTe with dimensions of 2 mm x 5 mm x 0.007 mm

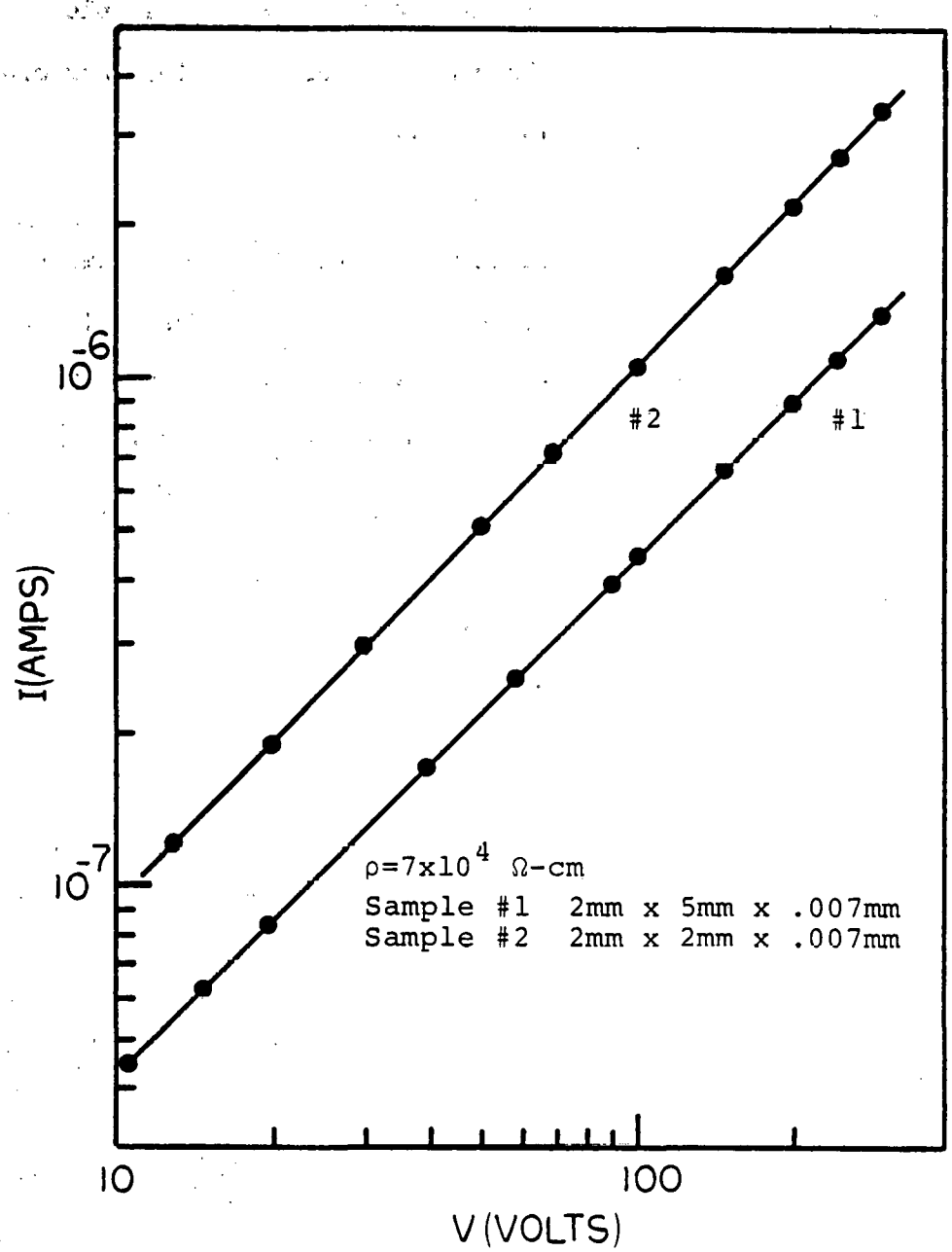

Figure 6. I-V Plot Showing the Linearity and Low Resistance of Contacts to CdTe Films

and 2 mm x 2 mm x 0.007 mm. It is noted that the resistance of the contacts was negligible because the current value for the 2 mm long sample was approximately 2.5 times larger than the 5 mm long sample. I-V characteristics were also symmetrical for applied (-) voltages.

a) Resistivity Measurements

Resistivity measurements were carried out on films that were electrodeposited at different rest potentials (E_{rest}). The variation of the resistivity with the rest potential is demonstrated in Fig. 7. The trend showing a decreased bulk CdTe resistivity at higher (-) potential is in accordance with the theory discussed by Panicker et al.[2] which says the material becomes more n-type as its Cd content increases. The bars indicate the range of resistivity values obtained for films that were prepared under similar conditions. Parts of this curve ($\rho<10^7$ Ω-cm) are also confirmed from the I-V measurements of Schottky barriers made on such films.

The variation of the resistivity with temperature was also examined. It was observed that this dependence is rather strong, a commonly observed phenomena in high resistivity CdTe crystals.[4,5,6,7] Fig. 8 is a semilogarithmic plot of conductivity vs. 1/T obtained for Sample #1. This plot indicates an activation energy of 0.3 eV. Other films with higher resistivities also gave activation energies in order of 0.4-0.5 eV.

Interpretation of these energy values is difficult without knowing the temperature dependence of the carrier mobilities in the material. The attempts to perform Hall effect measurements to get the mobility values had only partial success. High resistivities coupled with thicknesses in the order of a few microns gave Hall samples with excessive resistances. Resulting large offset voltages and drift problems did not usually allow

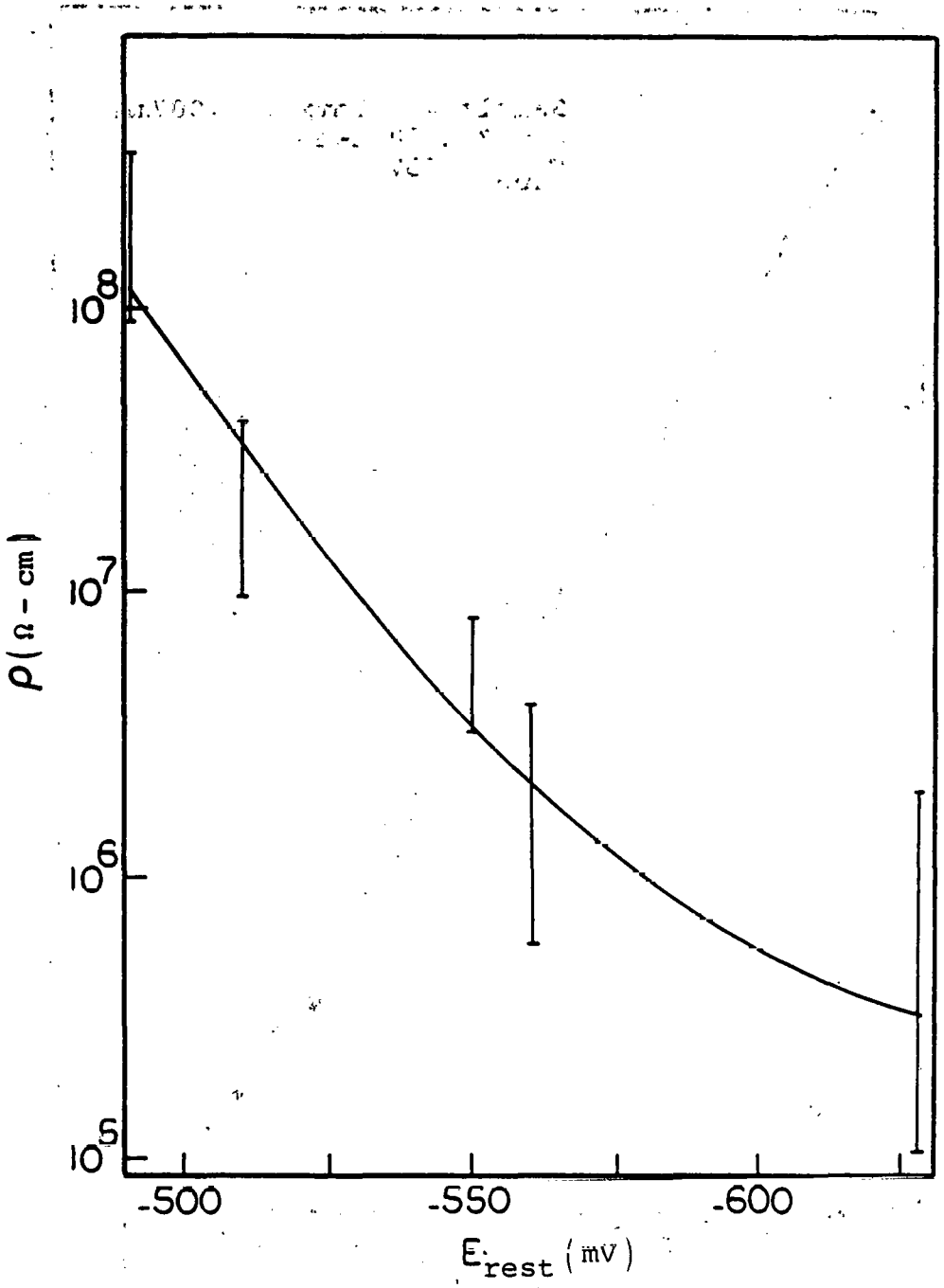

Figure 7. Resistivity of CdTe Films vs. E_{rest}

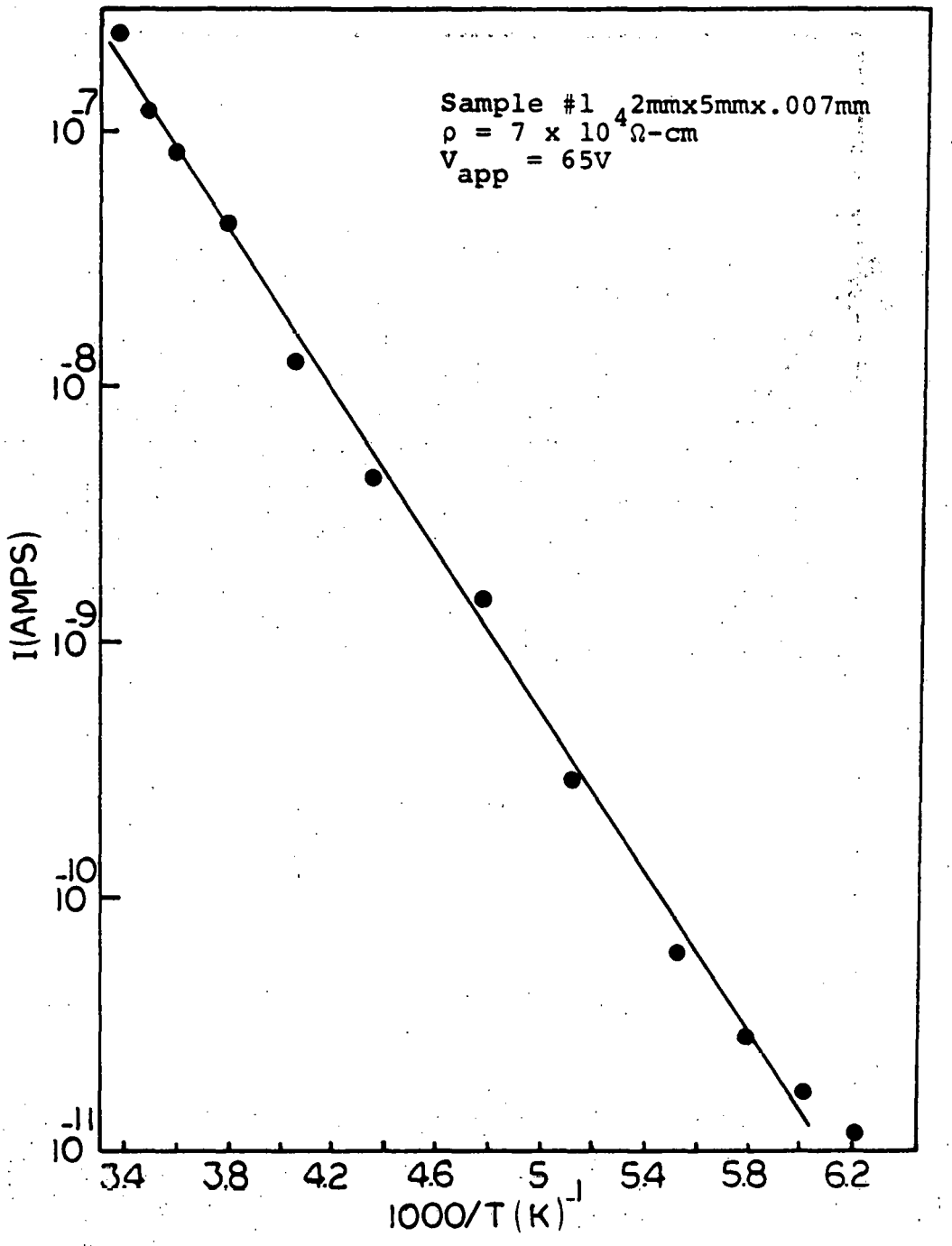

Figure 8. Current vs. 1/T for a CdTe Sample

the observation of small Hall voltages. The successful measurements performed on two different samples gave values in the range of 10-30 cm^2/V-sec for the electron mobilities. These values are reasonable for polycrystalline thin films of CdTe.

Although there are different models attempting to explain the high resistivity in CdTe thin films, all of them take into account the effects of native defects and native defect-impurity complexes giving rise to electrical compensation in the material. The presence of deep levels in our samples were confirmed by experiments that will be reported upon later in this report. There is no doubt that these centers have great influence on the electrical properties of our films.

b) Photoconductivity Measurements

Experiments made on electrodeposited CdTe layers mechanically peeled off their conductive substrates showed that this material is photosensitive. The results of such experiments are given below.

- Transient Measurements

The rise and the decay curves of photoconductive current were plotted using an X-Y recorder when the sample material was illuminated with a monochromatic light of λ = 0.7 μm. Fig. 9 shows the characteristic behavior of the rise and fall transients when the light is turned on or off suddenly. The important point to note is the excessive amount of time required for the current to settle at the dark value, a behavior typical of a material with trapping centers in the energy gap. These centers cause the long response times because they capture electrons (holes) and then re-emit them to the conduction (valence) band thus increasing the effective

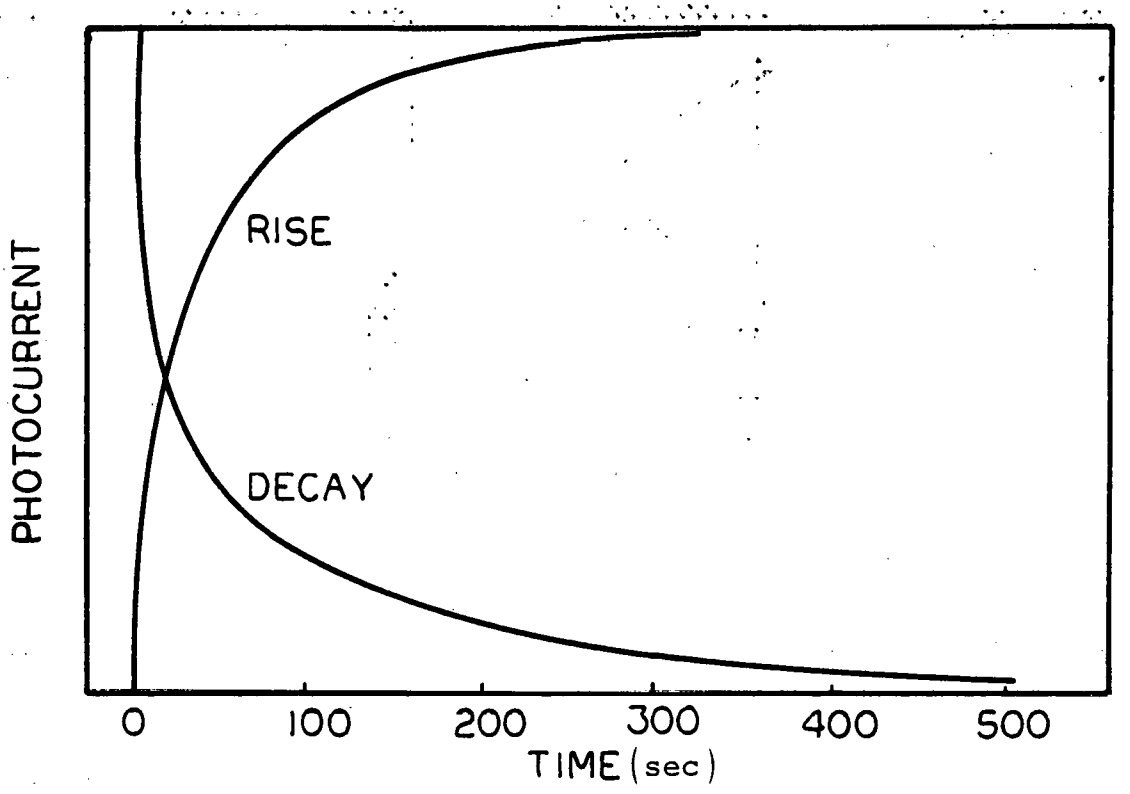

Figure 9. Transient Photoconductivity at Room Temperature

time spent by the free carriers in the conduction or valence bands. Of course these carriers eventually recombine at the recombination centers, and the current decreases.

The fact that the tail of the decay curve extends to minutes is indicative of the presence of very slow centers in electrodeposited CdTe layers. Presence of such centers was suggested earlier in our work by Kröger and Lehovec[8] as a result of the observed slow transients in Monosolar ITO/CdTe/Te devices they examined. The time dependence of the photoconductivity observed in our experiment can not be represented by a simple exponential which is expected for a single set of discrete trapping levels.[9]

This is commonly observed phenomena in II-VI compounds, the electrical characteristics of which are dominated by several deep levels in the energy gap.[10,11,12]

To be able to better resolve the fast portion of the decay curves, a high intensity pulsed dye laser was used, and the decay curves were observed using a fast oscilloscope. Dividing the curves into exponential portions, decay times ranging from microseconds to milliseconds were observed. However, there was still a fast decaying portion of the curve that could not be resolved with the equipment available. This decay represented a time of $<10^{-8}$ sec. This value can be taken as an upper limit for the lifetime in the material.

The information about minority carrier lifetimes in CdTe is scarce, and the existing data are not consistent due again to the well-known complexity of the point imperfections in CdTe. A lifetime of 10^{-9}-10^{-10} sec is a very acceptable value for our polycrystalline material considering the fact that same order of magnitude lifetimes are reported even for some single crystal CdTe material.

– Steady State Measurements

Steady state photoconductivity measurements were carried out using a set of bandpass filters and a variable intensity light source. Actual values of light intensity on the surface of the sample were measured by a DRC-2M Thermopile detector which was mounted near the sample. Fig. 10 shows a typical photoresponse spectra obtained from a rectangular sample (4 mm x 5 mm x .00125 mm) of electrodeposited CdTe film. Photocurrent values were measured at each wavelength by adjusting the incident illumination power to a constant value. This eliminated the problem one encounters

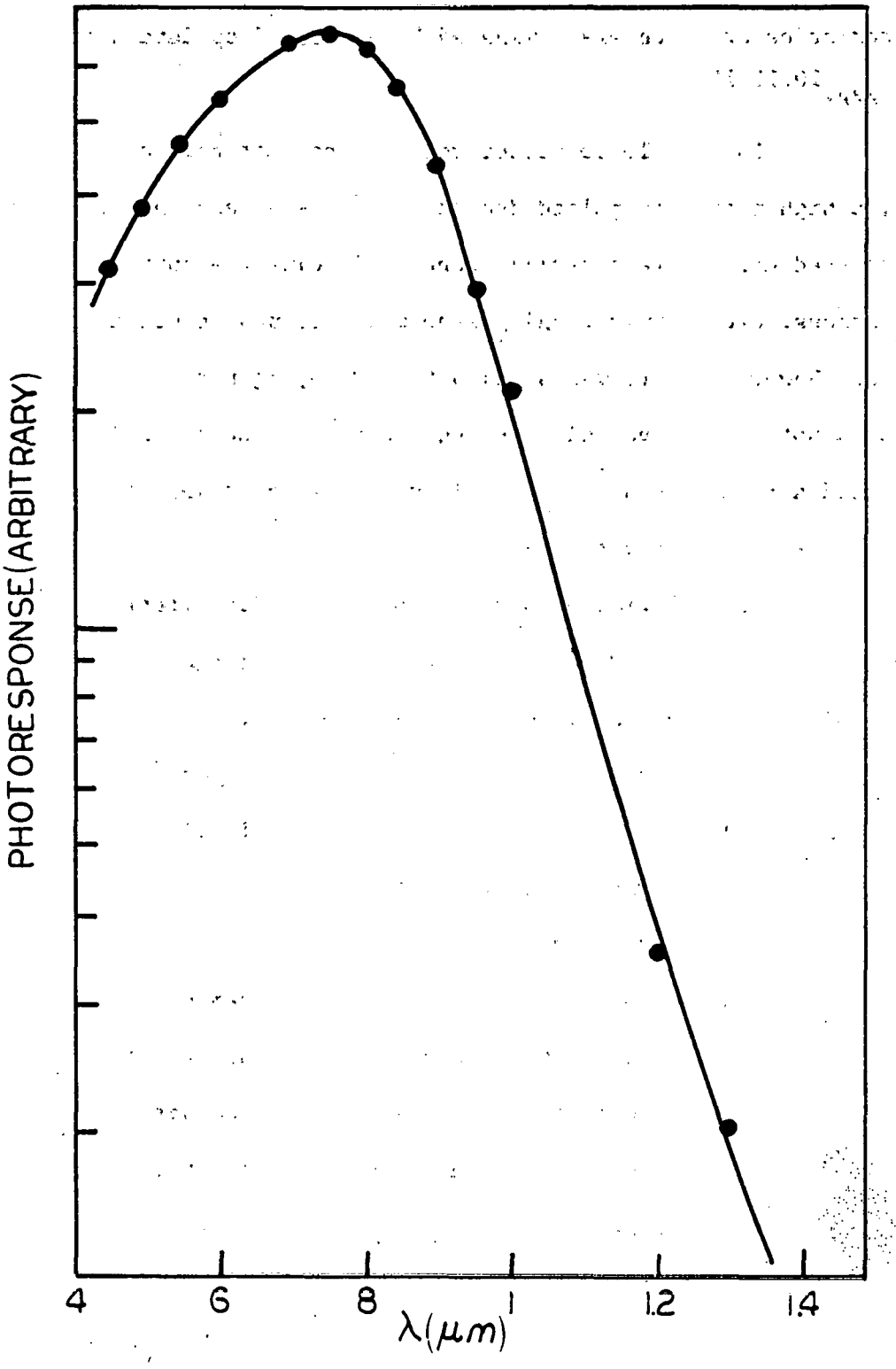

Figure 10. Photoresponse Spectra of CdTe Films

in normalizing the data taken at different intensities when the photocurrent does not change linearly with illumination intensity. This actually is found to be the case for electrodeposited CdTe. Fig. 11 shows the photocurrent vs. illumination intensity curves obtained for $\lambda = 0.75$ μm at two different temperatures. The shapes of these curves are invariant with respect to the bias voltage and indicate a sublinear dependence of the photo-generated current with respect to intensity. This dependence can be represented by:

$$I_{ph} \propto (\text{Intensity})^{n}, \; 0.5 \leq n < 1 \qquad (1)$$

Variation of the photogenerated carrier density with a power of I between 0.5 and 1 at low light intensities can be explained by postulating a trap distribution that extends over the small range of energies through which the quasi-Fermi level for electrons moves as the light intensity is increased.[13] Because of the high resistivity of the films, the above model suggests the presence of deep trap levels in our material that are at least 0.4 eV deep from the conduction band. The same model also qualitatively accounts for the decreased photocurrent at low temperatures. Because the temperature dependence of capture cross sections of these traps are unknown, a quantitative analysis was not possible.

Going back to Fig. 10 again, one can see that the spectral response of the films shows a broad peak around $\lambda = 0.75$ μm. The drop observed at very low wavelengths is indicative of surface recombination, while the observation of photocurrents for $\lambda > 1$ μm again confirms the presence of energy levels in the material.

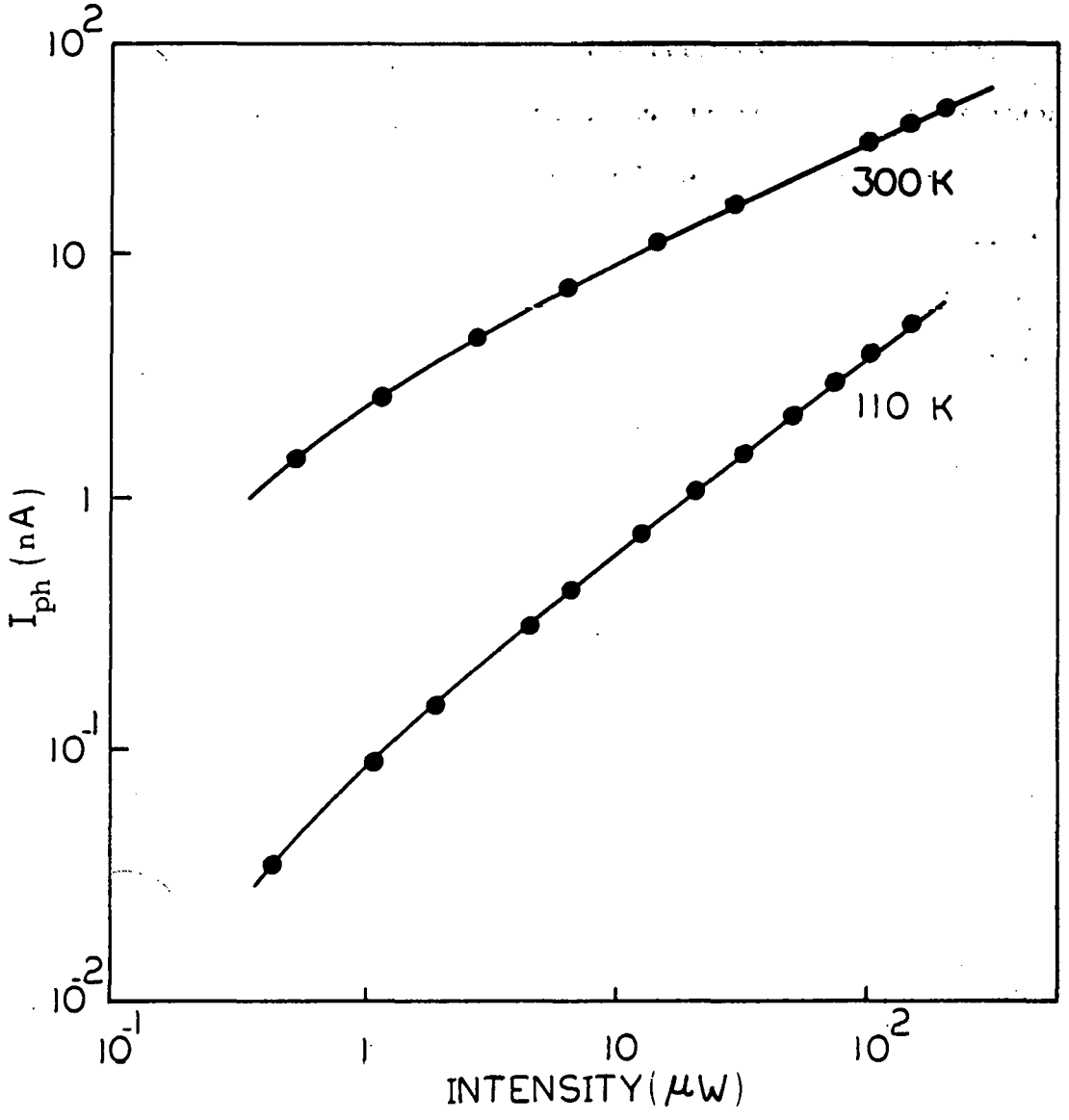

Figure 11. Variation of the Photocurrent with Illumination Intensity

V. DEVICES

Results of the experiments made using Schottky barrier devices will be reported in this section. Schottky barriers were prepared on different resistivity n-CdTe films by evaporation of Au or Al through shadow masks. Diodes obtained had rectification ratios as high as 10^4. The easy current directions indicated that the substrate materials (both Ni and ITO) acted as electron injecting contacts for the n-type films used. I-V and C-V measurements were performed on devices to gain information about the deep levels in high resistivity material.

1. Current Voltage and Capacitance Measurements of Schottky Devices on Very High Resistivity Films ($\rho \geq 10^7$ Ω-cm)

a. Current-Voltage Measurements

Current-voltage measurements of Schottky devices made on the highest resistivity CdTe films showed the characteristics of a space-charge-limited (SCL) current mechanism. Theory of SCL currents predicts that the space charge of the carriers injected into a diode from an injecting contact contributes to the current if the material's dielectric relaxation time is large compared to the transit time of these carriers. Analysis of space-charge-limited currents is a valuable tool in studying the defect levels in high resistivity materials, especially if the density of these traps is larger than the density of free carriers. In such cases, some useful methods like DLTS are not applicable. SCL currents have been observed in a variety of materials such as Si, Ge, CdTe, ZnTe, CdSe, CdS, ZnS, GaAs, SiC, KCl, etc., and they can be represented by the general equation[14]

$$J \alpha V^n \qquad (2)$$

where n is a constant which can be larger than or equal to 2 depending on the electronic properties of the material studies. Either metal/semi-insulator/metal or heterojunction structures can be used to study the SCL mechanisms.

In the case of one carrier injection and one dominant shallow trapping level, the equation (2) takes the form of:

$$J \simeq \Theta\varepsilon\mu \frac{V^2}{L^3} \tag{3}$$

where

μ is the mobility

ε is the permittivity of the material

Θ is the ratio of free-to-trapped charge density in the material and

L is the distance between the contacts.

It should be noted that a shallow trapping level is defined as a level which is above the Fermi level in the material. In high resistivity materials, the Fermi level must lie near the center of the band gap and these trap levels therefore are in a position normally referred to as "deep".

Θ is given by the equation:

$$\Theta = \frac{n}{n_t} = \frac{N_c}{gN_t} \exp\left(-\frac{E_t}{kT}\right) \tag{4}$$

where

N_c is the effective density of states in the conduction band

N_t is the trap density

E_t is the depth of the trapping level measured from the conduction band and

g is the degeneracy factor

n and n_t are free and trapped electron densities respectively.

The degeneracy factor g will not be included in the first order analysis that follows. Figure 12 shows the room temperature forward I-V characteristics of a Ni/CdTe/Au device. The thickness of the device is about 1 μm and the area of the gold contact is 1 mm^2. Easy current flow direction is from Au to the Ni contact. That is, the Ni is an injecting contact for electrons. Rectification ratios as high as 10^4 at 1 volt applied bias are observed. V^2 dependence of the current is observed for these devices for voltages greater than ~0.55 volts. The current in the V^2 region is strongly temperature dependent, suggesting that the dominant trapping level lies above the Fermi energy. Figure 13 shows the I-V characteristics of the device in the SCL region at various temperatures. The trap energy can be found from this temperature dependence according to Equation (4). Figure 14 shows a plot of the current at 1 volt applied voltage vs. 1/T. E_t is found to be 0.55 eV from the slope of this curve. The trap density calculated from Equation (4) and (3) is approximately $7x10^{15}$ using $N_c = 8x10^{17}/cm^3$ and E_t = 0.55 eV. A mobility of 1000 cm^2/V-sec is assumed in this calculation.

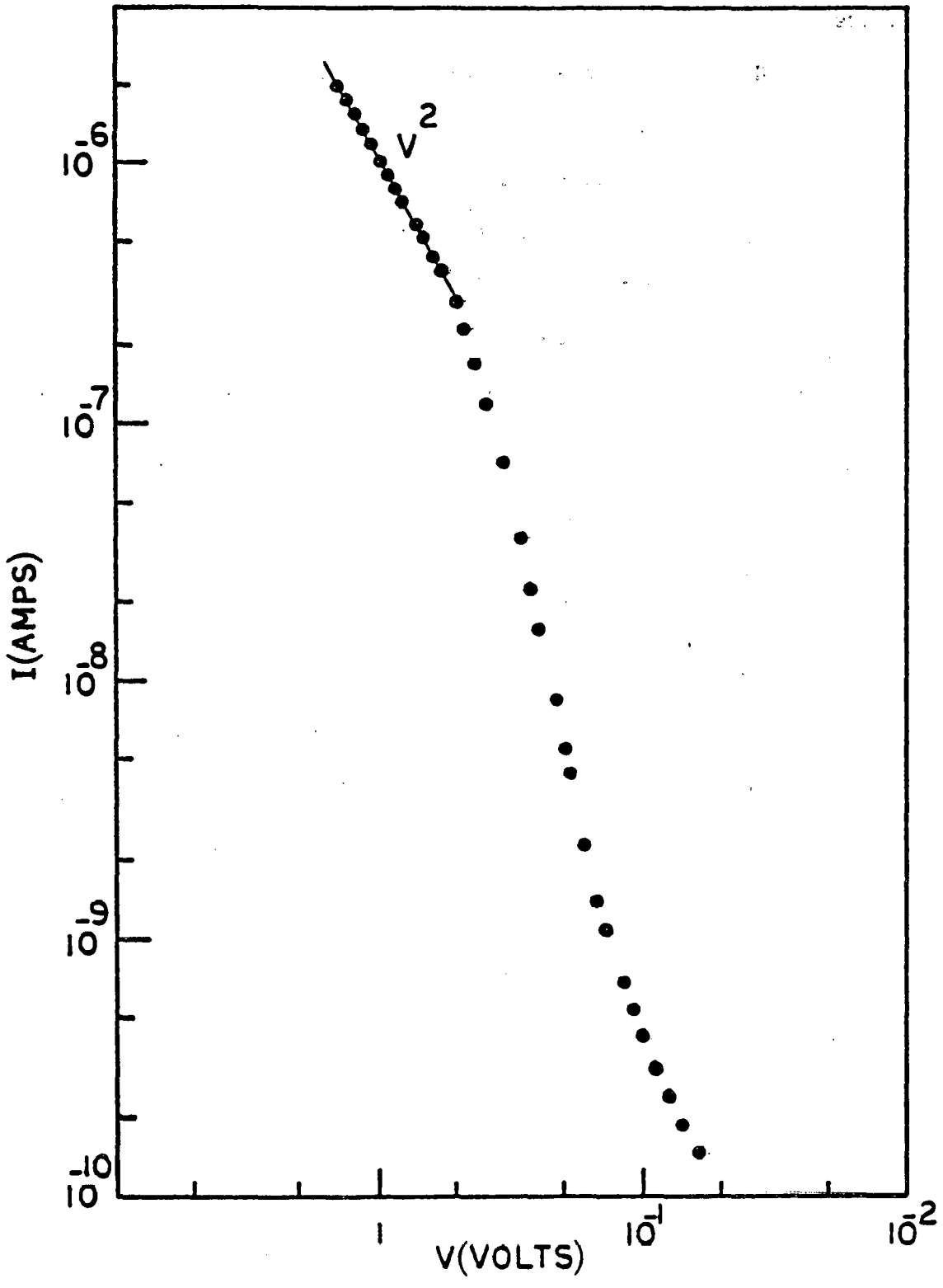

Figure 12. I-V Characteristics of a Ni/CdTe/Au Device Showing SCL Currents

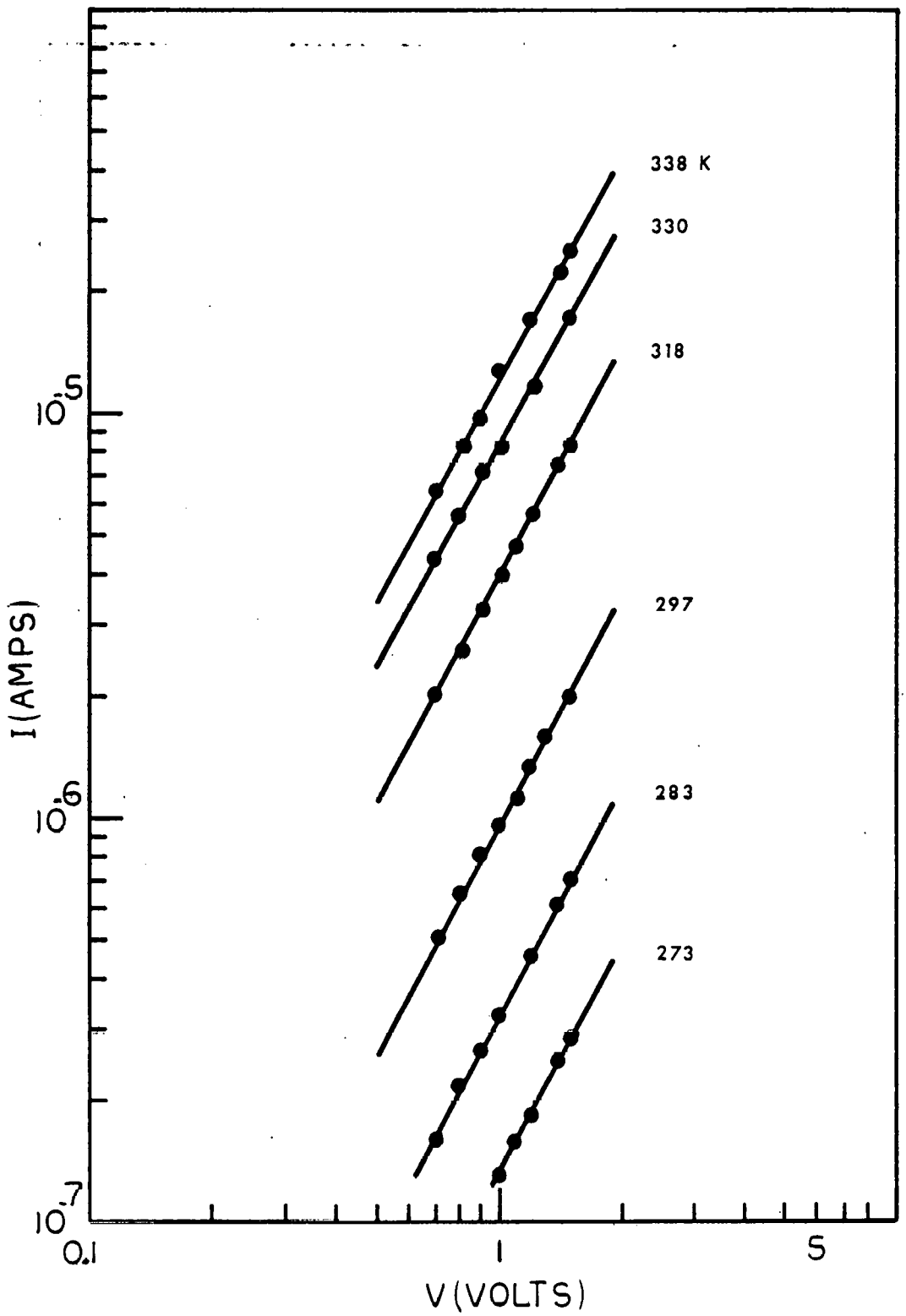

Figure 13. Temperature Dependence of the SCL Current in the V^2 Region

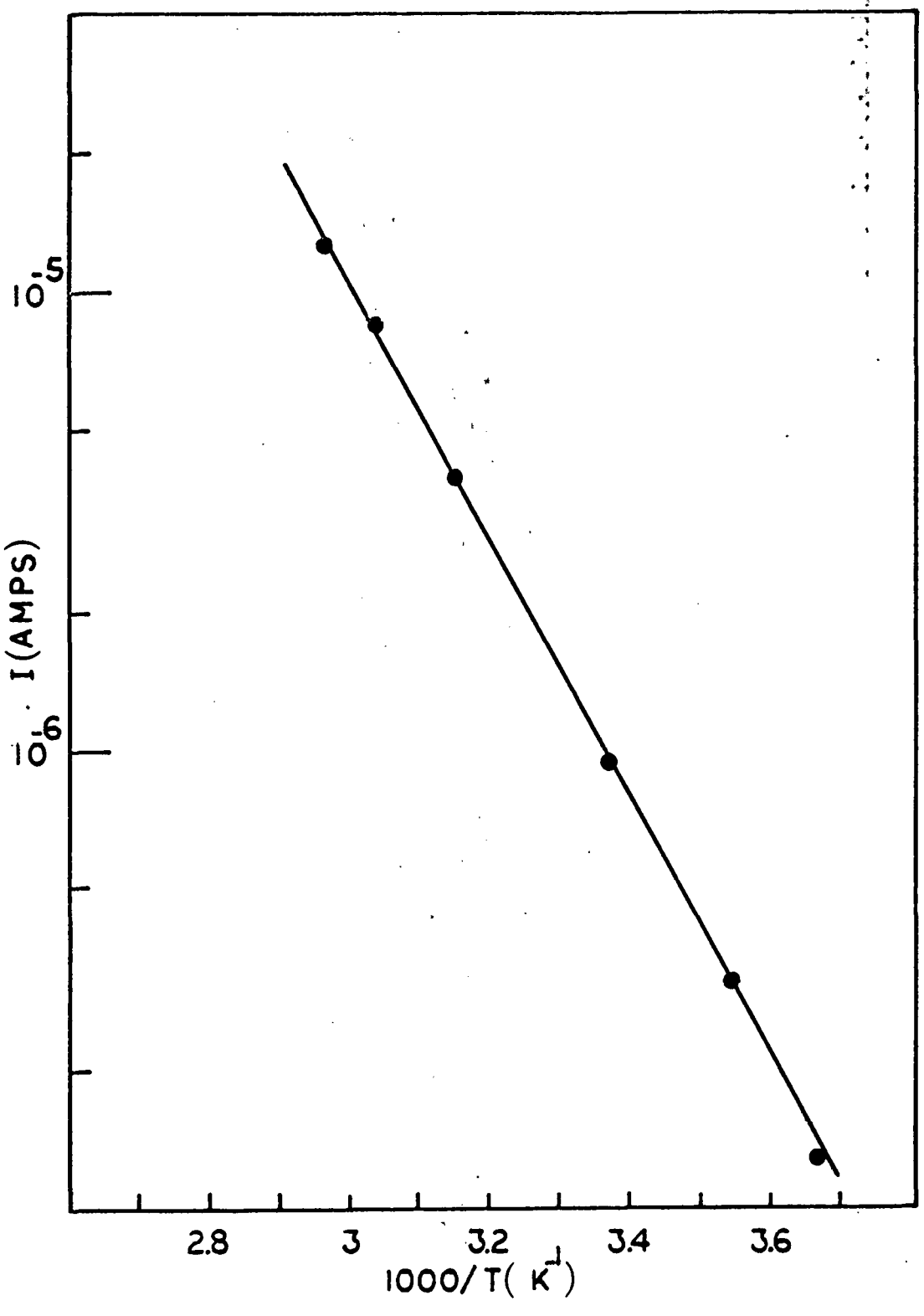

Figure 14. SCL Current at 1 Volt Applied Voltage vs. 1/T

The best way to distinguish between the single carrier space-charge-limited currents and other current mechanisms that may give rise to a V^2 current dependence is to determine the thickness dependence of the current and see if it follows Equation (3). Figure 15 shows the log-log plot of the current measured for a set of devices with different CdTe thicknesses. The dependence of the current on L^{-3} is observed from this figure within error limits of the thickness measurement. This confirms the single carrier injection assumption.

These findings are in good agreement with the reported values of CdTe trap energies measured by various techniques. Scharager et al.[15] found an electron trap at 0.55 eV from the conduction band using Temperature Stimulated Current (T.S.C.) data. A level of 0.58 eV was reported by Marfaing et al.[16] using a photocapacitance method. Rabin et al.[17] on the other hand, reported a value of 0.55 eV using their capacitance vs. frequency data. Energy levels at 0.65 eV[18], 0.53 eV[19], and 0.56 eV[20] were also reported using the analysis of SCL currents in high resistivity CdTe. A very recent investigation on evaporated CdTe[21] showed a distribution of trapping levels that start 0.52 eV below the conduction band and extend 0.62 eV. The method of measurement was SCL currents. The results of analysis of the capacitance measurements made on our devices will be presented in the next section. These results confirm the findings of the SCL current measurements of this section.

The reverse current of these devices can also be studied to reveal valuable information about the rectifying contact properties. The reverse currents are as low as 10^{-8} A/cm^2 at 1 volt. This demonstrates the good quality of these devices. The reverse current density values reported

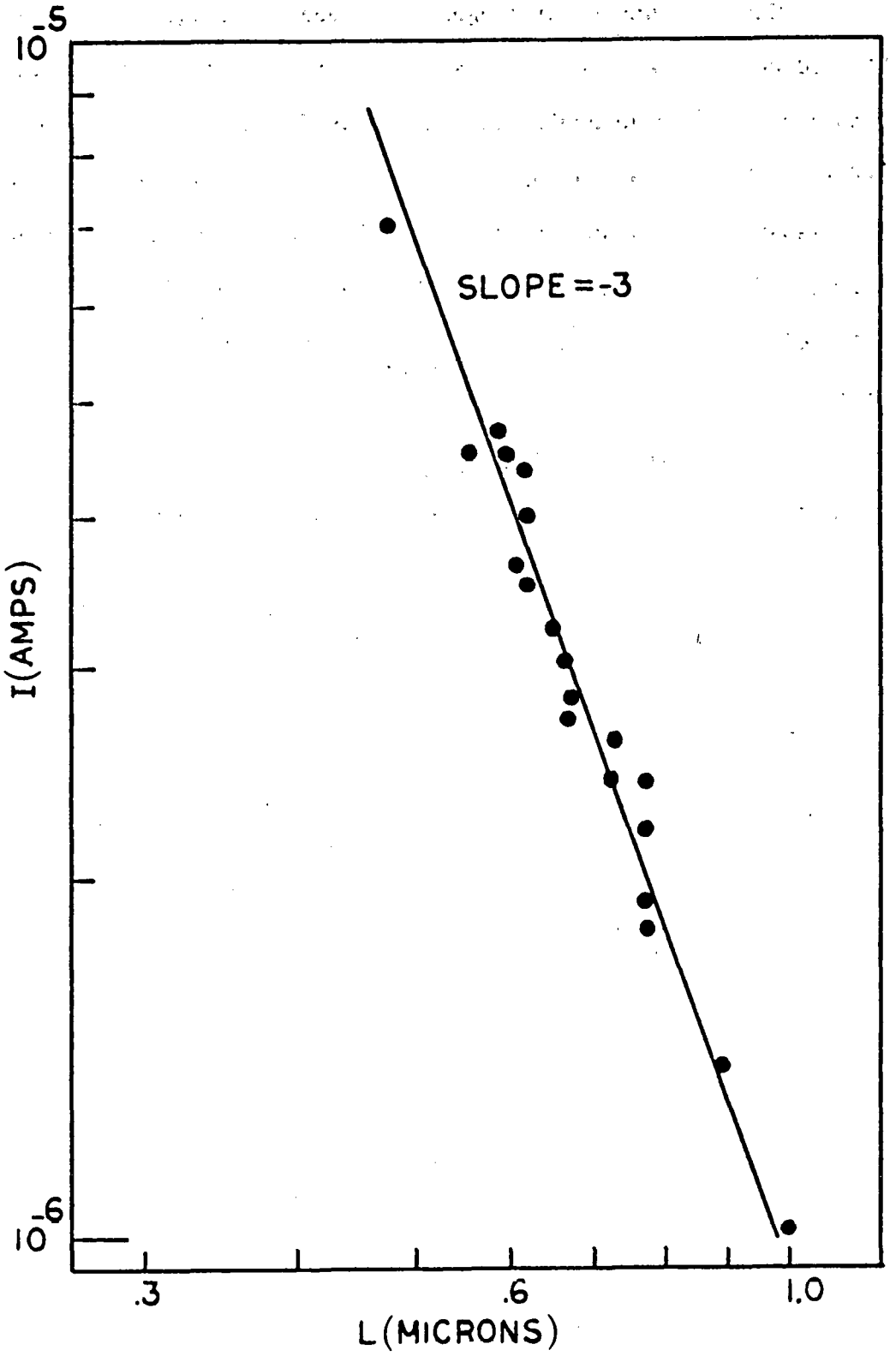

Figure 15. Thickness Dependence of the SCL Current

for any homo- or heterojunction using CdTe is 10^{-7}-10^{-10} A/cm^2, 10^{-9} being the typical value. Assuming a thermionic emission model then, the reverse saturation current should follow a relation:[22]

$$J = A^* T^2 \exp(-\frac{\phi_b}{kT}) \qquad (5)$$

where

A^* is the effective Richardson constant and

ϕ_b is the barrier height

In practical devices, however, the perfect saturation of the reverse current is not usually observed. Effects such as generation in the depletion region, leakage, and barrier lowering give rise to voltage-dependent reverse currents. Generation mechanism is especially important in devices produced on low lifetime materials such as II-VI compound semiconductors.

Figure 16 shows a semilogarithmic plot of the room temperature reverse current-voltage characteristics of two typical devices with areas 1 mm^2 and 2 mm^2. The barrier height can be determined from the temperature dependence of the reverse characteristics according to Equation (5). Figure 17 is a semilog plot of I/T^2 as a function of $1/T$ for device #1 at V=1 volt. The slope gives a barrier value of $\sim$0.8 eV. Experiments on other sets of devices gave barrier energy values ranging from 0.8 to 0.9 eV. This results is in good agreement with the previously reported CdTe/evaporated Au barrier heights of 0.7 eV[23] -0.86 eV[24]. The effective Richardson constant can also be calculated using the determined barrier value of 0.8 eV.

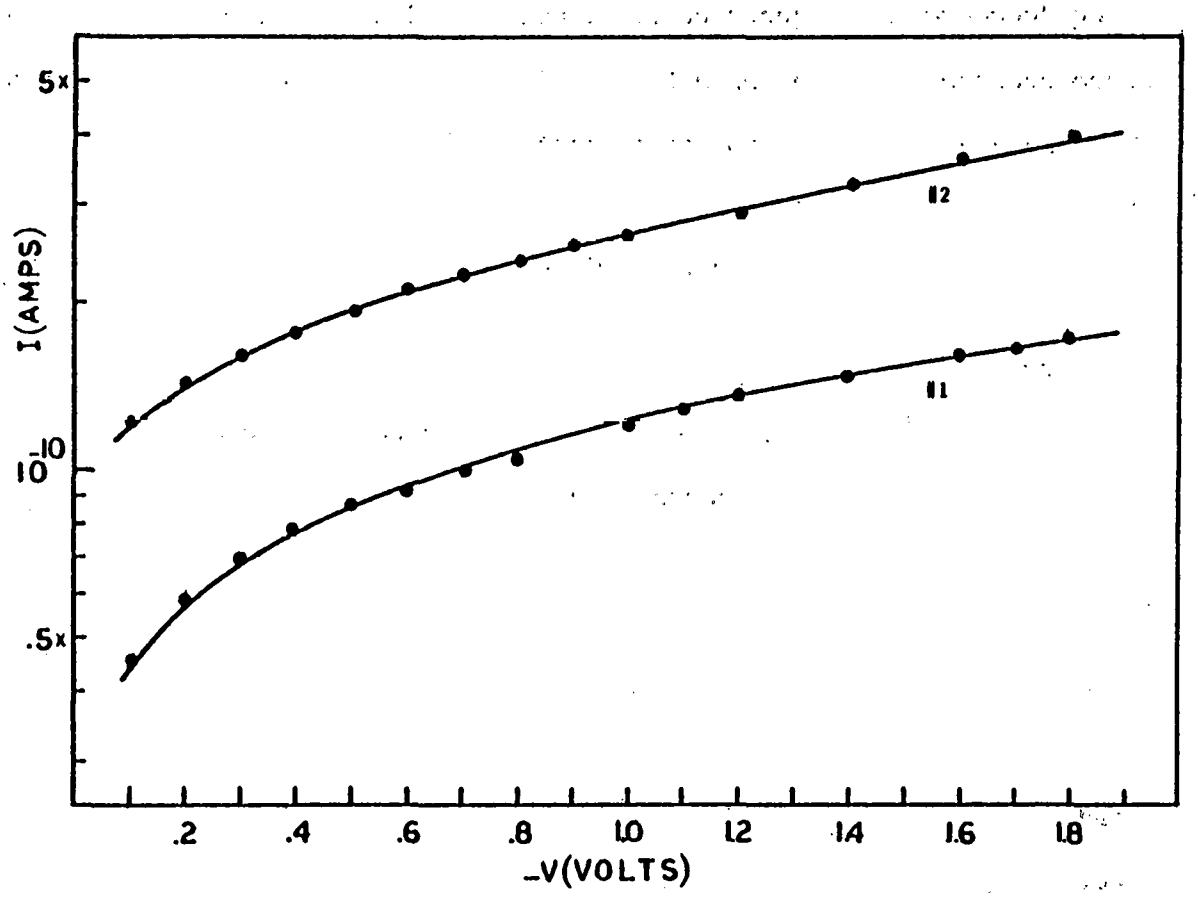

Figure 16. Reverse I-V Characteristics of Ni/CdTe/Au SCL Diodes

From Equation (5):

$$10^{-8} \simeq A^{*} (300)^{2} \exp -\left(\frac{0.8}{0.025}\right)$$

The value of A^{*} obtained from this relation ($9A/cm^2\text{-}K^2$) is extremely close to the theoretical value of $12A/cm^2\text{-}K^2$.

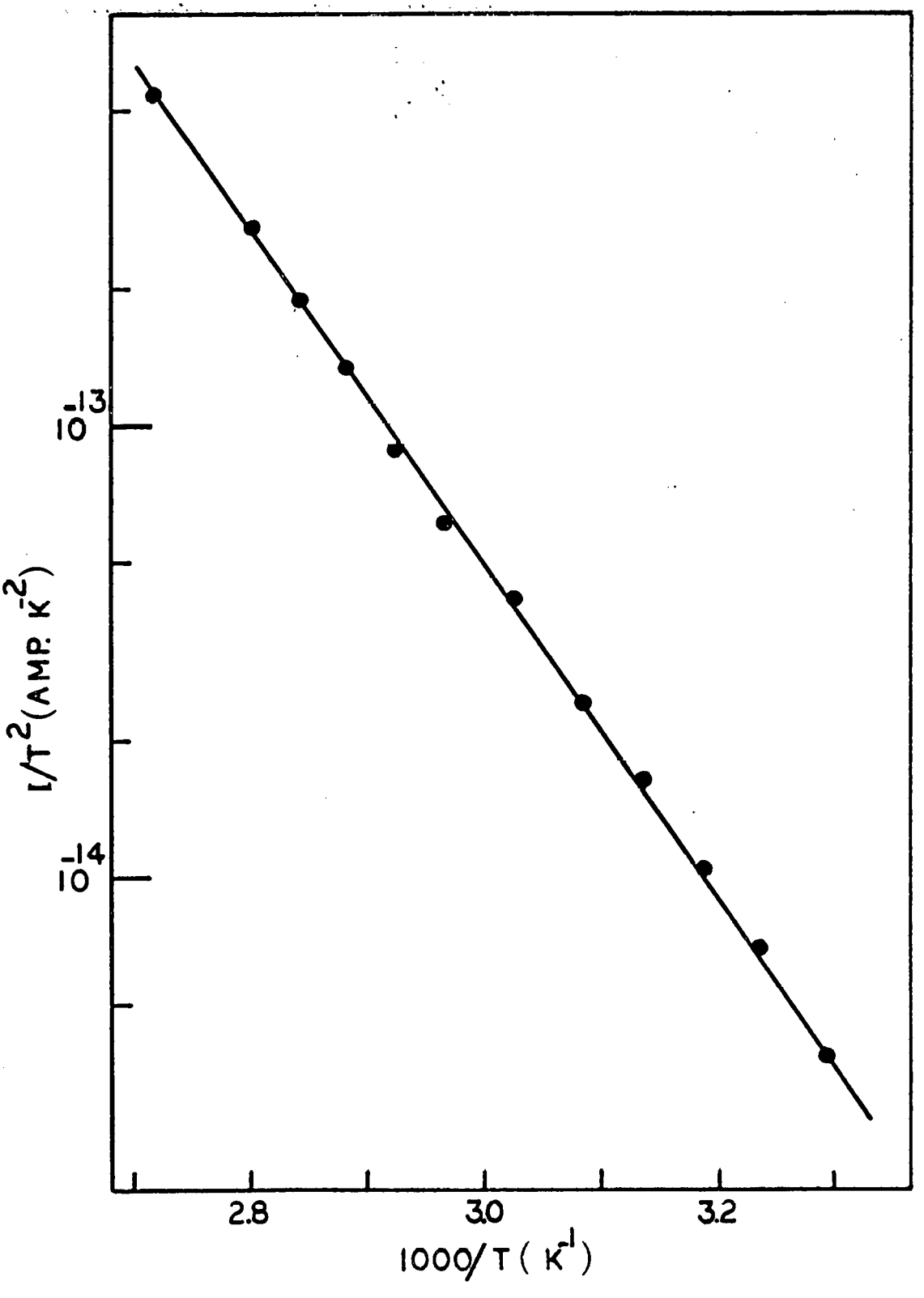

Figure 17. Reverse Current vs. 1/T for a SCL Diode

b. Capacitance Measurements

Capacitance measurements of the Schottky diodes made on high resistivity films ($\sim 10^7$ Ω-cm) show some very distinctive characteristics:

i) The value of the capacitance at low frequencies is quite large compared to a value one would expect for devices made on a high resistivity material.

ii) Although the capacitance decreases with the reverse bias, this dependence does not obey the familiar $C \propto (V_{bi} + V)^{-\frac{1}{2}}$ relationship which allows the simple deduction of V_{bi} and the doping density from the $1/C^2$ vs. V curves.

iii) The capacitance is a strong function of temperature and frequency.

iv) There are transient effects in the capacitance when the voltage across the device is changed suddenly.

All of the above characteristics are indicative of trapping levels in the material.

Fig. 18 shows a typical C-V characteristics of our Schottky diodes measured at various different frequencies. It is observed that

$$C \propto V^{-m}, \quad 0 < m < 0.5 \tag{6}$$

where the value of m decreases with increasing frequency. m = 0.2 at 100 Hz. The capacitance becomes independent of the applied voltage for large frequencies, and it behaves as a planar capacitor with an electrode spacing equal to the thickness of the film. Effect of frequency and temperature on

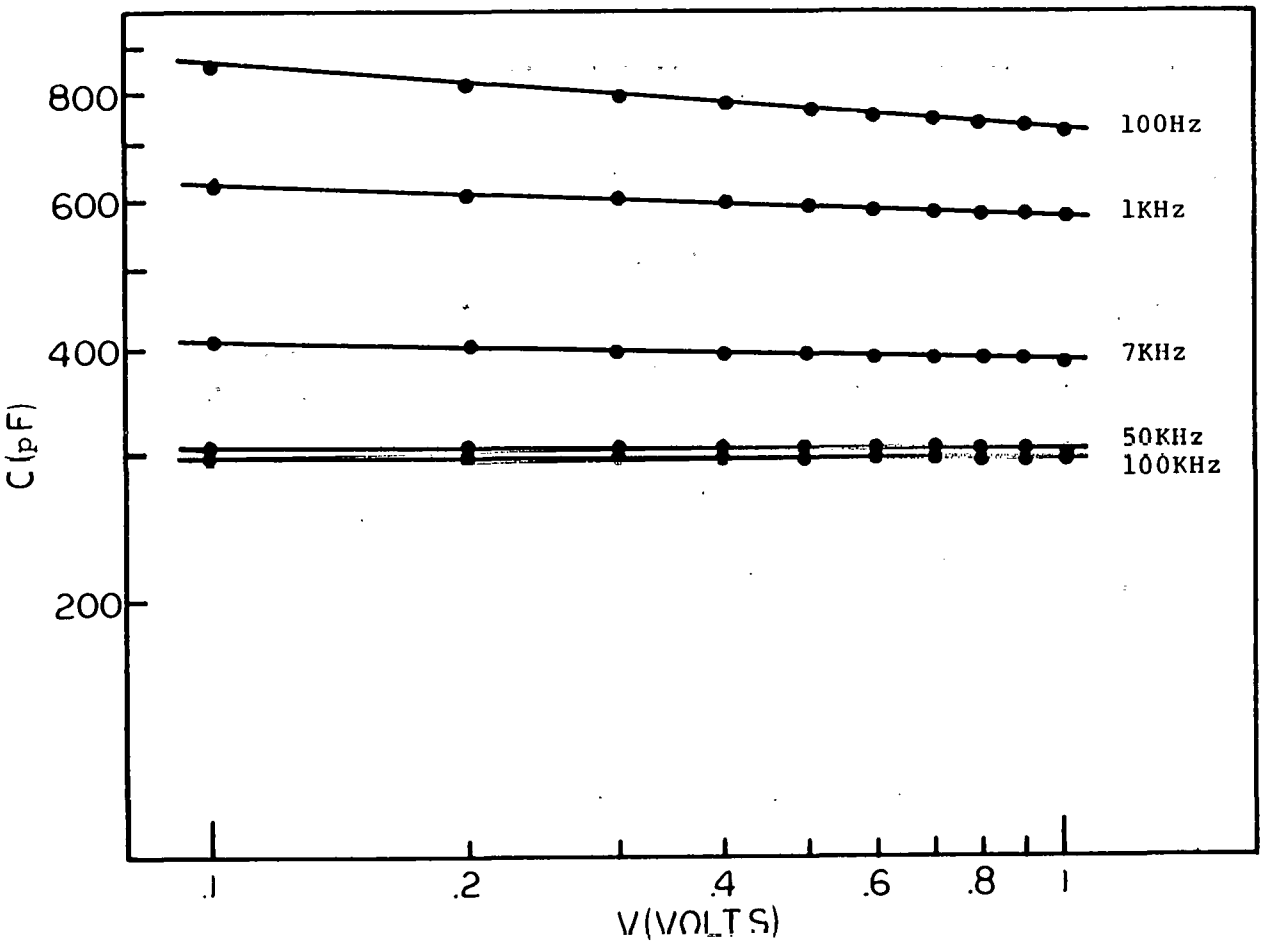

Figure 18. Capacitance vs. Reverse Bias Voltage for a Ni/CdTe/Au Device

the measured capacitance is demonstrated in Fig. 19 which shows the zero bias capacitance vs. frequency for a device. It is observed that while the capacitance values are a strong function of the temperature at low frequencies, this dependence decreases as frequency increases. Eventually C becomes a constant independent of temperature as well as frequency.

Observation of a capacitance in the form of Equation (6) is previously reported by several authors[17,25,26,27,28] for p-n junctions and Schottky barriers produced on high resistivity CdTe. There are different

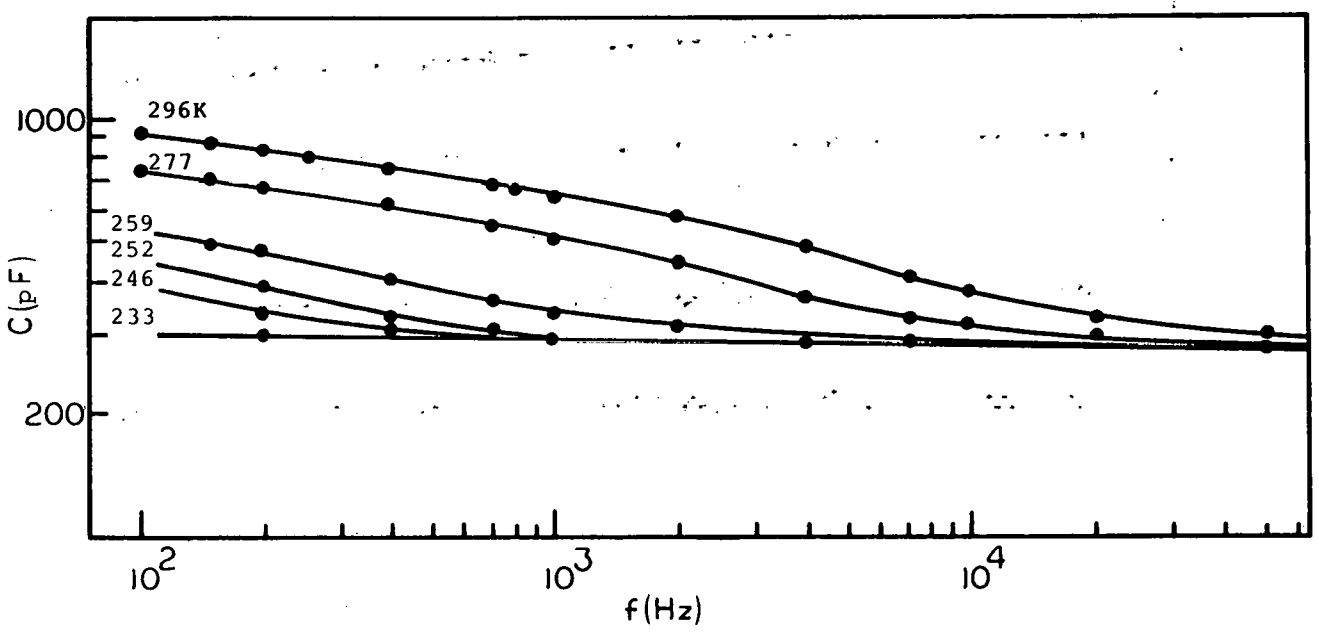

Figure 19. Zero Bias Capacitance vs. Frequency Characteristics of a Ni/CdTe/Au Device at Different Temperatures

models to explain such phenomena in materials with trapping levels. The model proposed by Schibli and Milnes[29] takes into account the case where the density of the deep traps exceeds the density of shallow level impurities. The energy band and charge diagram of a metal/n-CdTe device with a dominant electron trapping level are drawn in Fig. 20. A low frequency, small signal voltage applied to this device gives rise to a charge increment near the edge of the depletion region. As the frequency of the signal is increased, the charge increment (q_f) moves into the bulk because of the limited ability of deep levels to follow the signal. Therefore, overall capacitance can be represented by the series combination of a frequency independent capacitance (C_{dc}) and a frequency dependent capacitance (C_f).

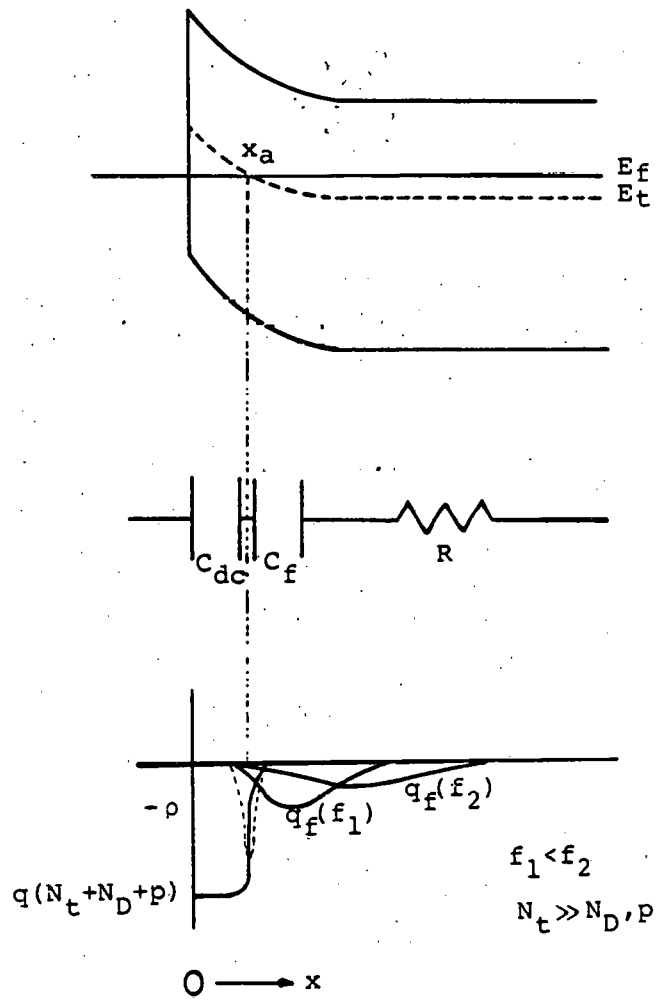

Figure 20. The Model of a Schottky Barrier with Large Deep Level Concentration

The total capacitance then is:

$$\frac{1}{C} = \frac{1}{C_{dc}} + \frac{1}{C_f} \tag{7}$$

where

$$C_f = \left(\frac{2\varepsilon q^2 N_t}{kT} \frac{\omega_1}{\omega}\right)^{\frac{1}{2}} \tag{8}$$

and

$$\omega_1 = C_n n_1 = C_n N_c \exp\left(-\frac{qE_t}{kT}\right) \tag{9}$$

N_t is the trap density, E_t is the trap depth and C_n is the electron capture probability of the traps. These equations are valid for:

$$\frac{1}{\tau} = (n+n_1)C_n \ll \omega \ll \frac{1}{\varepsilon\rho} \tag{10}$$

where

ρ is the resistivity

ε is the permittivity

We can see from the above equations that the region where Equation (8) holds for our devices extends to relatively low frequencies, because the resistivity of our material is high giving rise to a larger τ. This explains the behavior of the C vs. frequency curves in Figure 19. It should be noted that the capacitance saturation ($C = C_{dc}$) region is not very distinct even at 100 Hz. Therefore, we measured the C_{dc} value using a

lock-in amplifier at frequencies as low as 10 Hz. The value thus obtained for C_{dc} is 1300 pF. Using this value and equation (7) C_f as a function of frequency is calculated and plotted in Figure 21. It is observed that the frequency dependence of C_f is stronger than that of C and this dependence is very close to the theoretical prediction of $f^{-\frac{1}{2}}$. Deviation from the theory at high frequencies can be attributed to the fact that the capacitance is approaching the high frequency asymptotic value, namely the geometrical capacitance. Because the resistivity of the material is high, this asymptotic value is reached at relatively low frequencies. Using Equations (8) and (9), we can now find the trap depth from the temperature dependence of the frequency dependent capacitance. Figure 22 shows the C_f vs. 1/T curves for three different frequencies. From the slopes of these curves, a trap depth of .56 eV is calculated. This value is very close to the value obtained from SCLC measurements and it most probably belongs to the same trapping levels because the preparation conditions of the films were similar. The trap density can be found using Equation (8) and the relation:

$$\omega_1 = \frac{kT}{q} \frac{\omega_b}{4V_j} \tag{11}$$

where

ω_b is the frequency where $C_f = C_{dc}$ and

V_j is the total D.C. voltage across the junction

In our case V_j is just the built-in voltage and f_b is about 800 Hz. Using $V_{bi} = 0.3V$, ω_1 is found to be in the order of 105. Using this value of ω_1

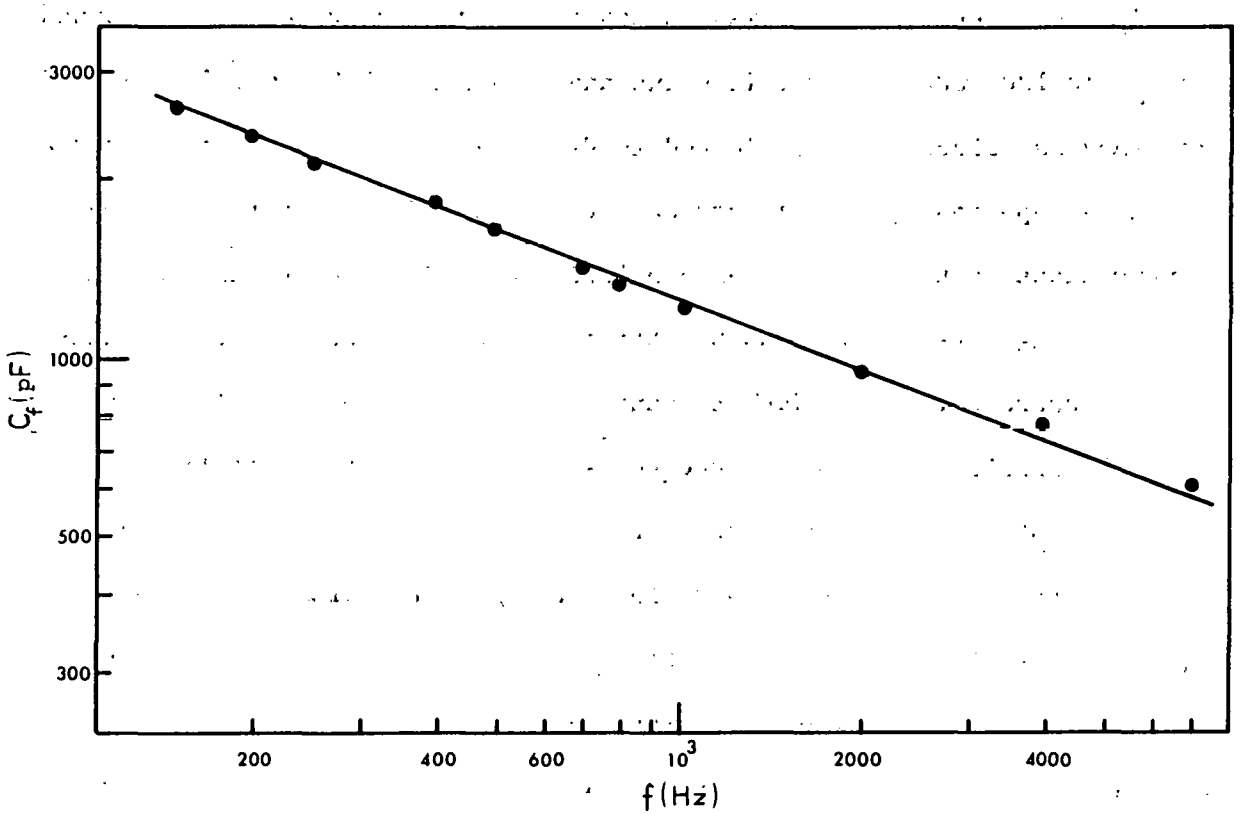

Figure 21. Frequency Dependent Capacitance (C_f) vs. Frequency

electron capture probability of the traps can be calculated from Equation (9). At room temperature:

$$n_1 = 8\text{x}10^{17} \exp\left(-\frac{0.56}{0.025}\right) \approx 1.5\text{x}10^8/\text{cm}^3$$

$$c_n = 105 \;/\; (1.5\text{x}10^8) \approx 7\text{x}10^{-7}$$

Taking $v_{th} = 10^7$ cm/sec for the electrons, the capture cross section is:

$$\sigma_n = 7 \times 10^{-14} \text{ cm}^2$$

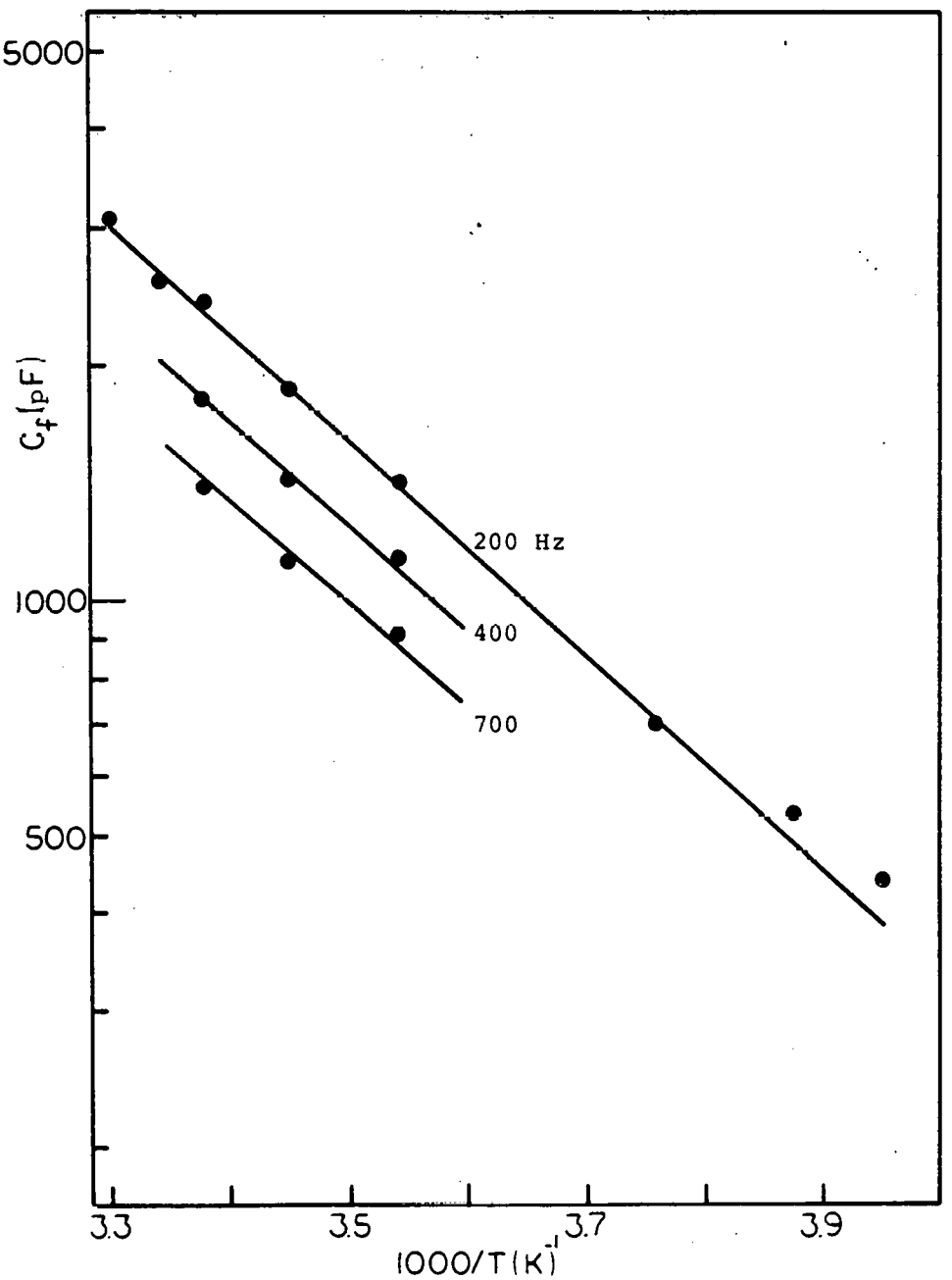

Figure 22. Temperature Dependence of C_f

The trap density is found to be about 3 x 10^{16} /cm^3 using the value of C_f at 400 Hz (C_f = 1800 pF). Now we can go back and calculate the trap density from C_{dc}.

$$C_{dc} = \frac{\varepsilon A}{W} \tag{12}$$

where

ε is the dielectric constant

W is the depletion width and

A is the area of the device

$$1300 = \frac{.02}{W} \qquad W = 0.15\ \mu m$$

Again taking V_{bi} = 0.3V, N_t can be calculated:

$$W = \left(\frac{2\varepsilon V_{bi}}{qN_t}\right)^{\frac{1}{2}}$$

$$N_t = 1.7 \times 10^{16}$$

This value is in agreement with the value found using C_f. The determined trap density and energy depth of the traps are in close agreement with the SCLC measurements. The value of the capture cross section suggests that the traps are positively charged. The capacitance measurements correlates well with the results of Rabin et al.[17] who measured a trap level at E_t = 0.55 eV with density of $N_t = 6x10^{15}(cm)^{-3}$ in undoped n-CdTe which was prepared by zone melting. Their method was similar to that used in this study.

The results of the two last sections again stress the importance of point defects in CdTe films. It should be noted that the trap levels observed in these experiments are usually attributed to Cd interstitials and/or vacancy-impurity complexes.

2. Electrodeposited CdTe Solar Cells

Schottky barrier solar cells were produced by evaporating transparent gold contacts through shadow masks onto freshly deposited CdTe films of 0.6-1 micron thickness. Both ITO coated glass and metallized glass were used as substrates. The first structure has the convenient feature that light can be shined from both sides of the cell. A brief etch (1-2 seconds) in aged 1% Bromine Methanol was also employed for some devices. Most of the cells studied are 2 mm^2 but larger devices were also produced without shorting problems. Figure 23 shows the short circuit density values, corrected for reflection, measured for several of these devices vs. the rest potential, E_{rest}, of the films. The illumination intensity was 85 mW/cm^2 in these measurements. The observed improvement in the current at high negative E_{rest} values is in agreement with the findings of Section IV. At lower potentials the increased resistivity of the film and the resulting change in contact resistance adversely effect the device performance. The same degradation was also observed in the open circuit voltage and fill factor. Figure 23 indicates the solar cell performance of a series of films made from a single plating solution under various deposition potentials. The devices whose characteristics will be examined in the next sections were produced on low resistivity films, ($\rho<10^6$ Ω-cm) that were prepared at high ($-E_{rest}$) values.

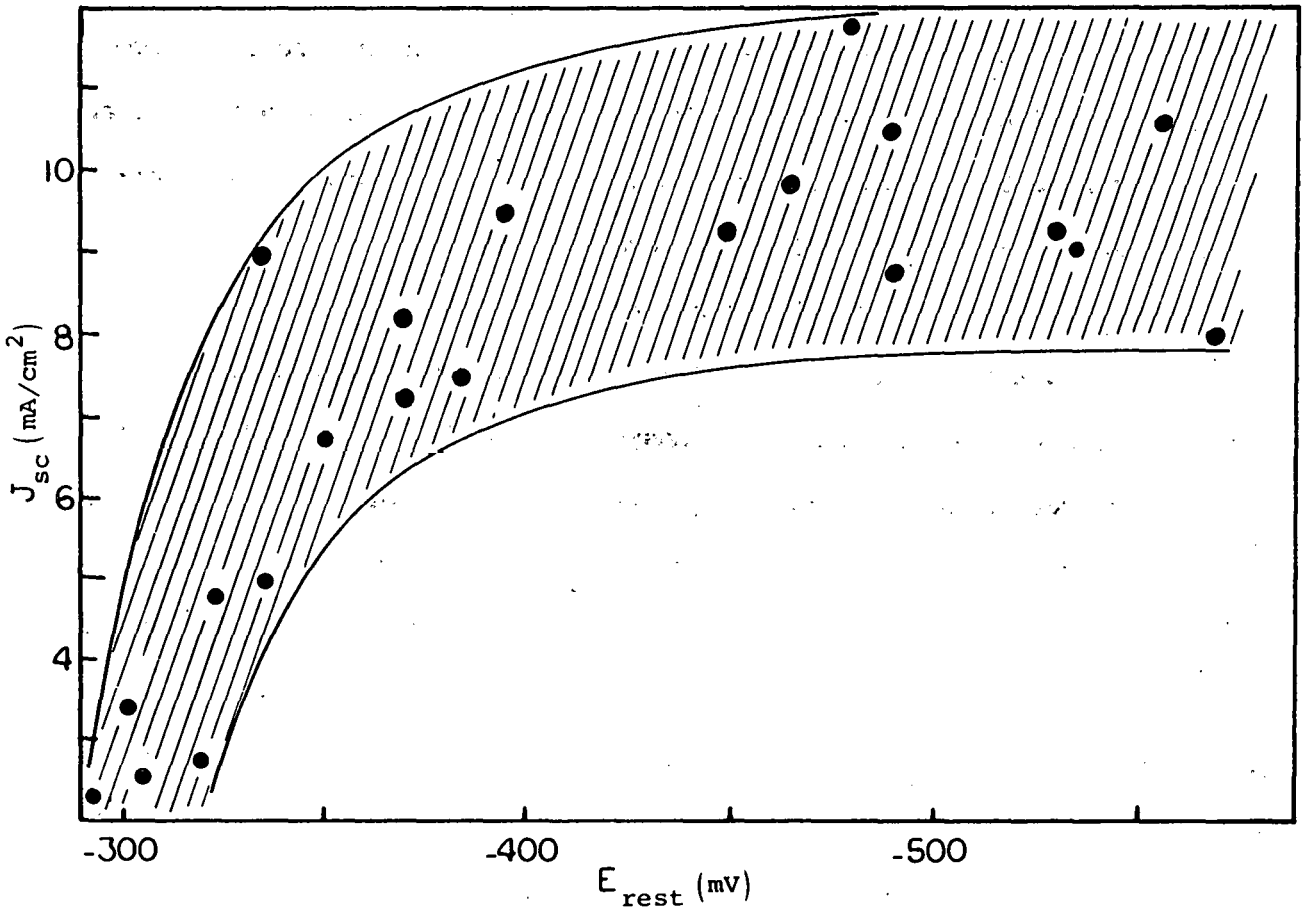

Figure 23. J_{sc} vs. E_{rest} for Electrodeposited CdTe Cells

— Dark I-V Characteristics of the Schottky Barrier Solar Cells

The I-V characteristic of a Schottky barrier is given by the familiar expression:

$$J = J_o \left[\exp\left(\frac{qV}{nkT}\right)-1\right] \qquad (13)$$

where

J_o is the reverse current density and

n is the diode factor.

For an ideal diode n takes the value of 1. But for devices where the generation-recombination in the depletion region is important, n is a number between 1 and 2. There are, of course, other effects,[22] such as an interfacial oxide, image force lowering of the barrier and series resistance, which can give rise to a diode factor between 1 and 2.

For an ideal Schottky J_o is given by the equation:

$$J_o = A^* T^2 \exp(-\frac{\phi_b}{kT}) \tag{14}$$

In a Schottky device where the generation-recombination in the depletion region is the dominant mechanism, the reverse current density is given by:[30]

$$J_{ro} = \frac{qn_i W}{2\tau_r} \tag{15}$$

where

n_i is the intrinsic carrier concentration

W is the depletion width and

τ_r is the lifetime in the depletion region

The generation recombination current is important for high barriers, for material of low lifetime, at low temperatures and at low forward-bias voltages. Frequent observation of large n factors at room temperature for p-n junctions, Schottky barriers and heterojunctions prepared on single crystal and polycrystalline CdTe is a result of the relatively low lifetimes in such materials.

Figure 24 shows the dark I-V characteristics of a ITO/n-CdTe/Au device at three different temperatures. It is observed that the room temperature curve can be represented by a diode equation in the form of Equation (13). The diode factor, n, is 1.9 for V<0.2 volts and 1.6 for 0.2<V<0.4. This indicates the pronounced effect of recombination in the depletion region. Other devices also gave n values ranging from 1.3 to 1.9. The temperature dependence also agrees with this mechanism. The sharp deviation from linearity for forward voltages larger than 0.4 is due to the series resistance of the bulk material and the contact resistance.

Because it was determined that generation-recombination is important in these devices, Equation (14) cannot be used to find the barrier energy. Instead, Equation (15) can supply information about the lifetime in the material. Taking the extrapolated intercept of the forward characteristics and the current axis, one obtains a value for the lifetime of:

$$\tau_r \simeq 8\times10^{-10} \text{ sec.}$$

Intrinsic carrier concentration was taken to be $n_i = 10^7/cm^3$ in this calculation. The depletion width was found from the low frequency capacitance and it was about 0.3 μm.

— Light I-V Characteristics of the Schottky Barrier Solar Cells

The open circuit voltage (V_{oc}) of a solar cell is related to the short circuit current density (J_{sc}) by the equation:

$$V_{oc} = \frac{nkT}{q} \ln\left(\frac{J_{sc}}{J_o} + 1\right) \qquad (16)$$

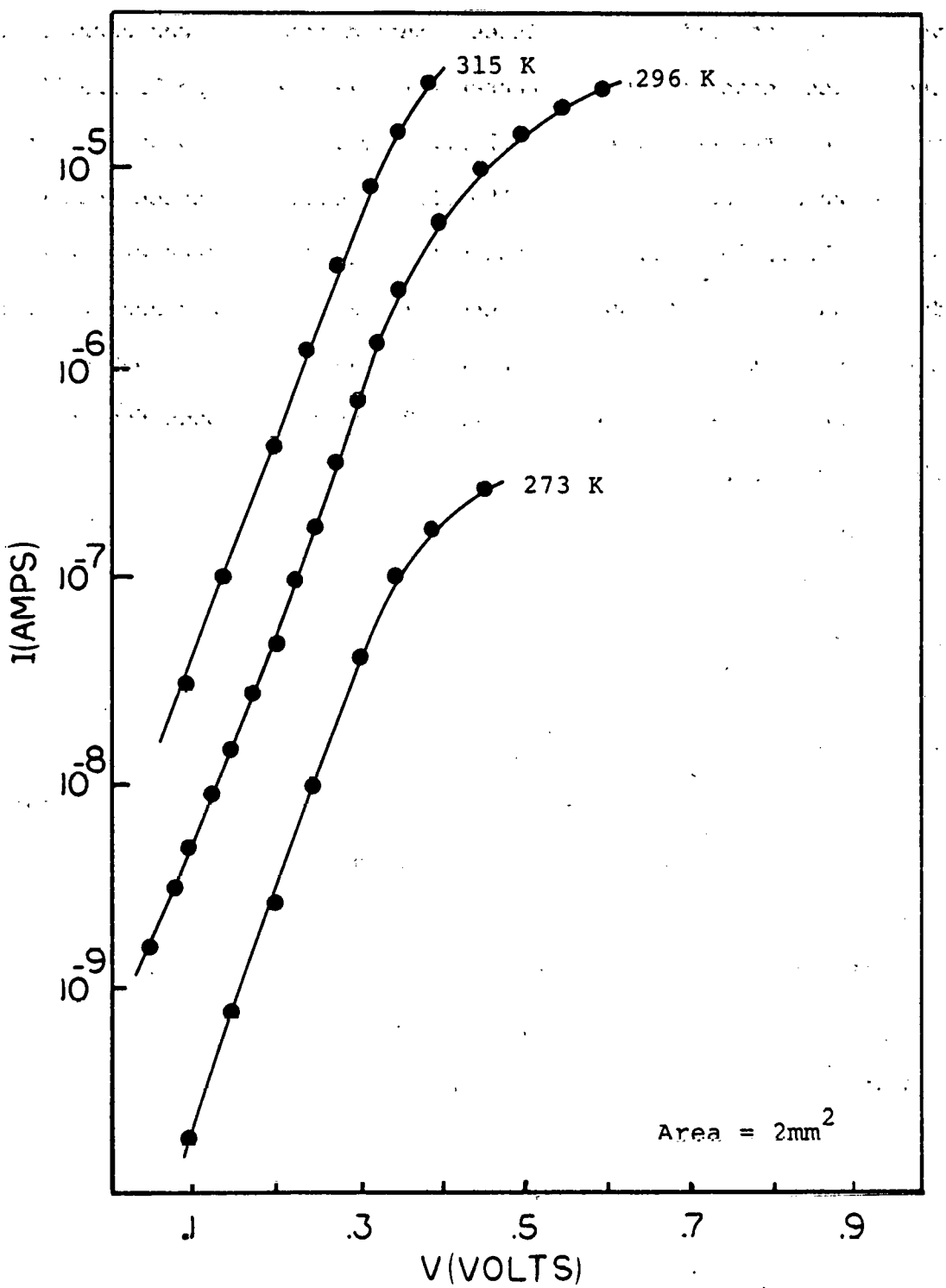

Figure 24. Dark I-V Characteristics of ITO/n-CdTe/Au Solar Cell

This relation suggests that one can obtain the value of n by plotting V_{oc} vs. log J_{sc} at various intensities. Such a procedure was carried out for the device whose dark I-V characteristics were given in Figure 24. Figure 25 shows the result at λ = 0.7 μm. The observed linear behavior is in accordance with Equation (16). The diode factor n is calculated from the slope. It is found to be 1.8 which is in good agreement with the value obtained from the dark I-V measurements. The I_o value obtained by extrapolating the log I_{sc} vs. V_{oc} curve to V_{oc} = 0 line is approximately $6x10^{-10}$A. This value of I_o also agrees with the value found from dark I-V characteristics.

In addition to the original $CdSO_4$-based electrolyte a second and newer bromide-based electrolyte was also used to prepare films. pH of both of the solutions was around 2 and the deposition temperature was about 90°C. A distinct difference was observed between the characteristics of the solar cells produced on two types of films. While the sulfate-based cells showed the highest V_{oc} values the bromide-based cells had improved fill factor and short circuit current density. Figure 26 demonstrates this observation. Reasons for this behaviour are under investigation and the aim is to bring together the favorable aspects of two processes.

The following Table 6 lists electrical characteristics of typical cells made in both types of electrolytes.

TABLE 6

Electrical Characteristics of Typical Cells

Cell#	V_{oc}(V)	I_{sc}(μA)	F.F.
PP-233*	0.23	108	0.49
PG-220*	0.23	80	0.46
PG-221*	0.28	85	0.45
PP-232*	0.32	130	0.41
PP-242*	0.32	90	0.50
PP-236*	0.33	85	0.49
PP-231*	0.33	115	0.54
PP-241*	0.38	64	0.49
IS-36N	0.39	40	0.45
IS-38N	0.39	50	0.45
PP-309*	0.39	95	0.55
IS-24N	0.48	50	0.40
PP-448A	0.53	50	0.40

Active area of the cells is about 0.015 cm^2. The measurements were made using a light source with 85 mw/cm^2. Cells* were plated in bromide electrolytes. Others were plated in $CdSO_4$.

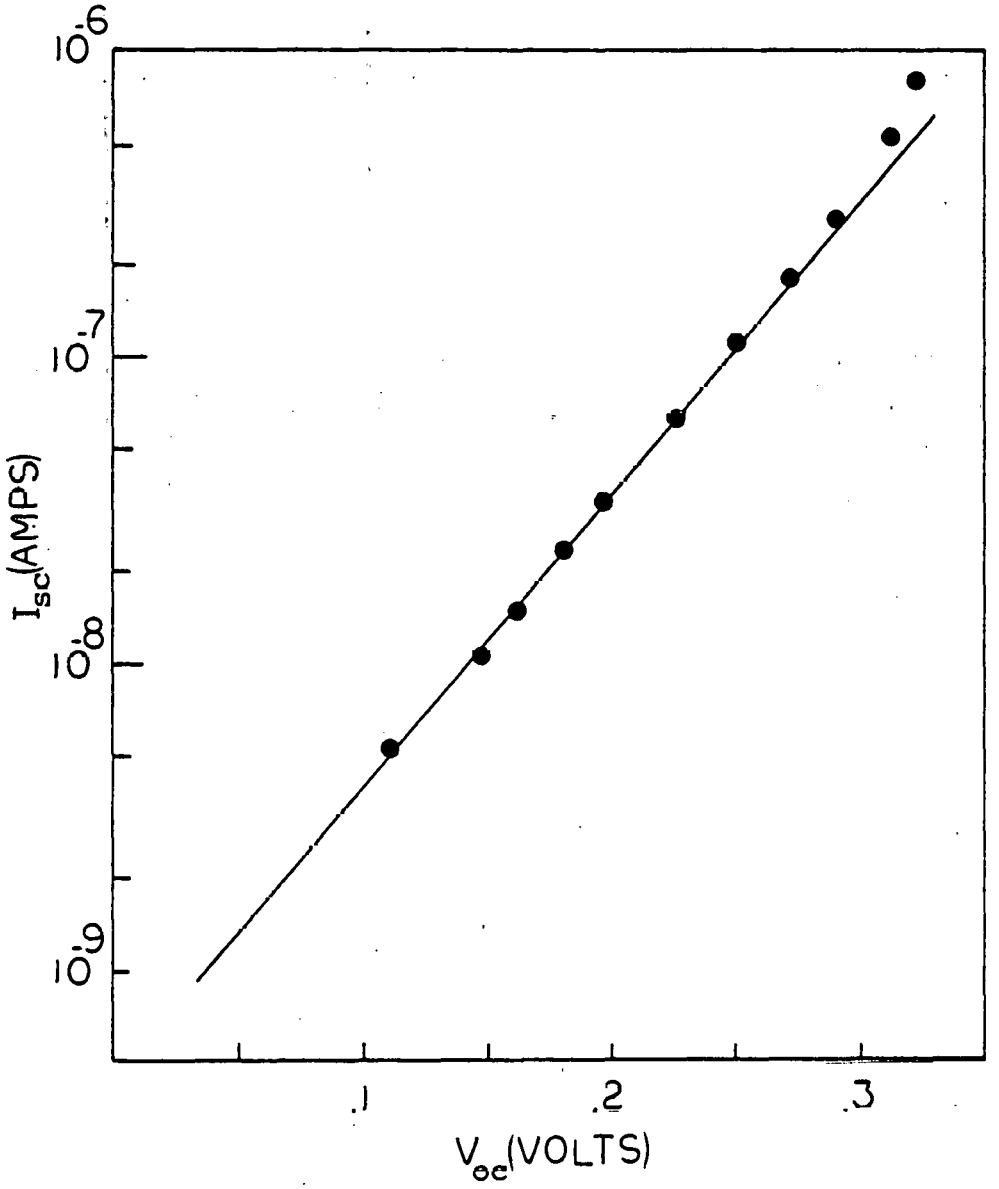

Figure 25. Log I_{sc} vs. V_{oc} Curve for an ITO/n-CdTe/Au Solar Cell

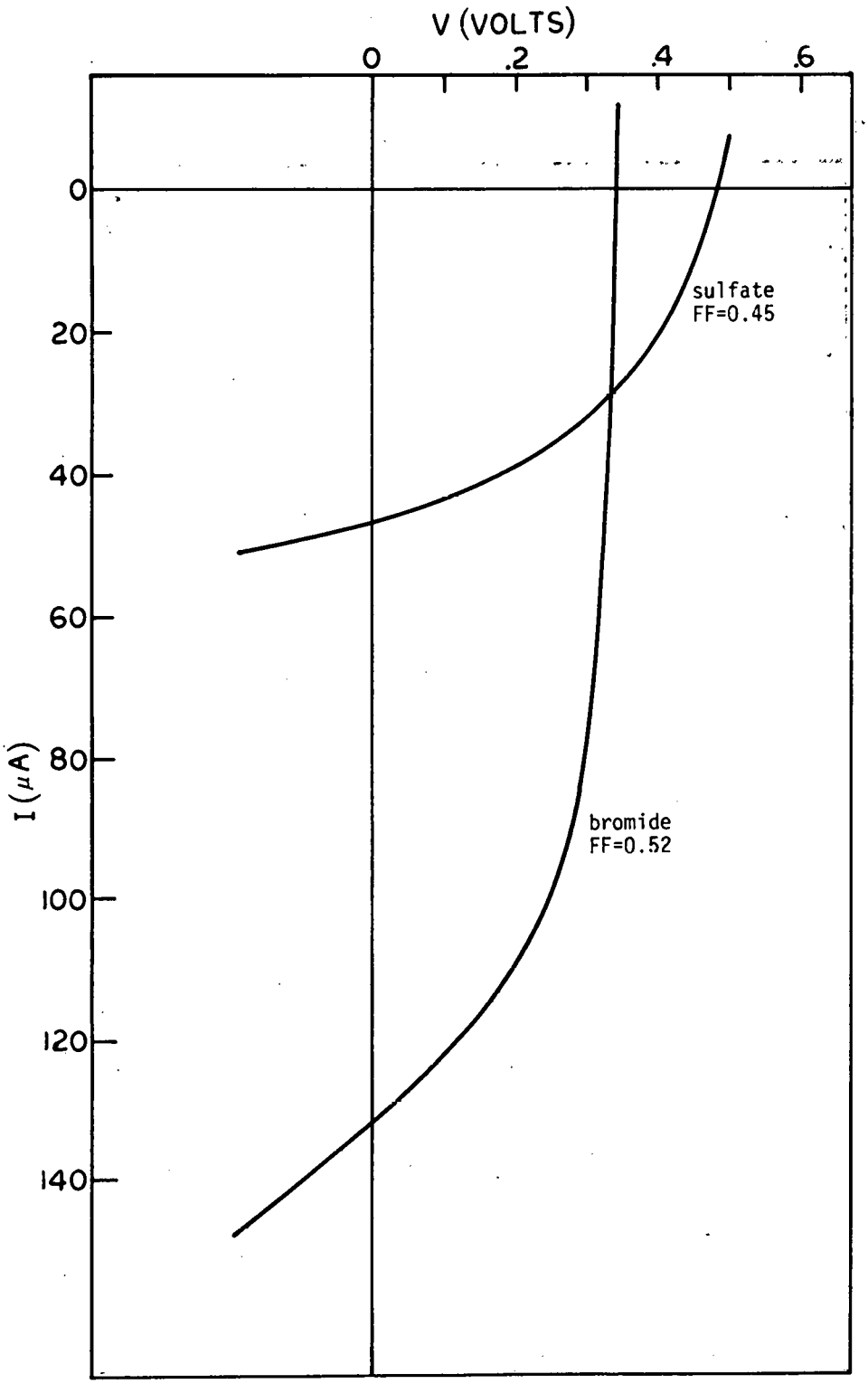

Figure 26. Light I-V Characteristics of Bromide-based and Sulfate-based Solar Cells

VI. PREPARATION OF TRANSPARENT CONDUCTING OXIDE FILMS

To be able to have a better control of the electrical and optical properties of the substrate ITO an in-house effort of preparing ITO films was initiated. Good quality films were obtained by a novel Activated Reactive Evaporation method. Results are summarized below:

Transparent electrically conducting thin films of various oxides (e.g., SnO_2, In_2O_3, In_2O_3(Sn) and Cd_2SnO_4) have attracted considerable attention in the recent years because of their technological importance. Apart from their potential use in various common applications such as transparent electric heaters for aircraft windows, antistatic coatings on instrument panels, these coatings are becoming an integral part of many sophisticated optoelectronic devices. To date, the best transparent conducting films are obtained either by chemical vapor deposition (hydrolysis of chlorides or pyrolysis) or sputtering (reactive sputtering or sputtering from an oxide target). The status of various conducting oxide coatings, prepared by different techniques has been summarized recently by Vossen[31] and Haacke[32]. This section reports on the preparation of high optical quality transparent conducting films of In_2O_3 and Sn-doped In_2O_3 films by a novel activated reactive evaporation technique.

Figure 27 shows schematically the experimental set-up. An oil diffusion pump equipped with a liquid N_2 trap was used to achieve a base pressure of $<2 \times 10^{-6}$ torr. A resistively heated tungsten/tantalum source was used for evaporating In or In-Sn Alloys. The substrates were mounted on a substrate table and can be maintained at temperatures ranging from 25 to 500°C. A mixture of Ar + O_2, used as a reactive gas was bled into

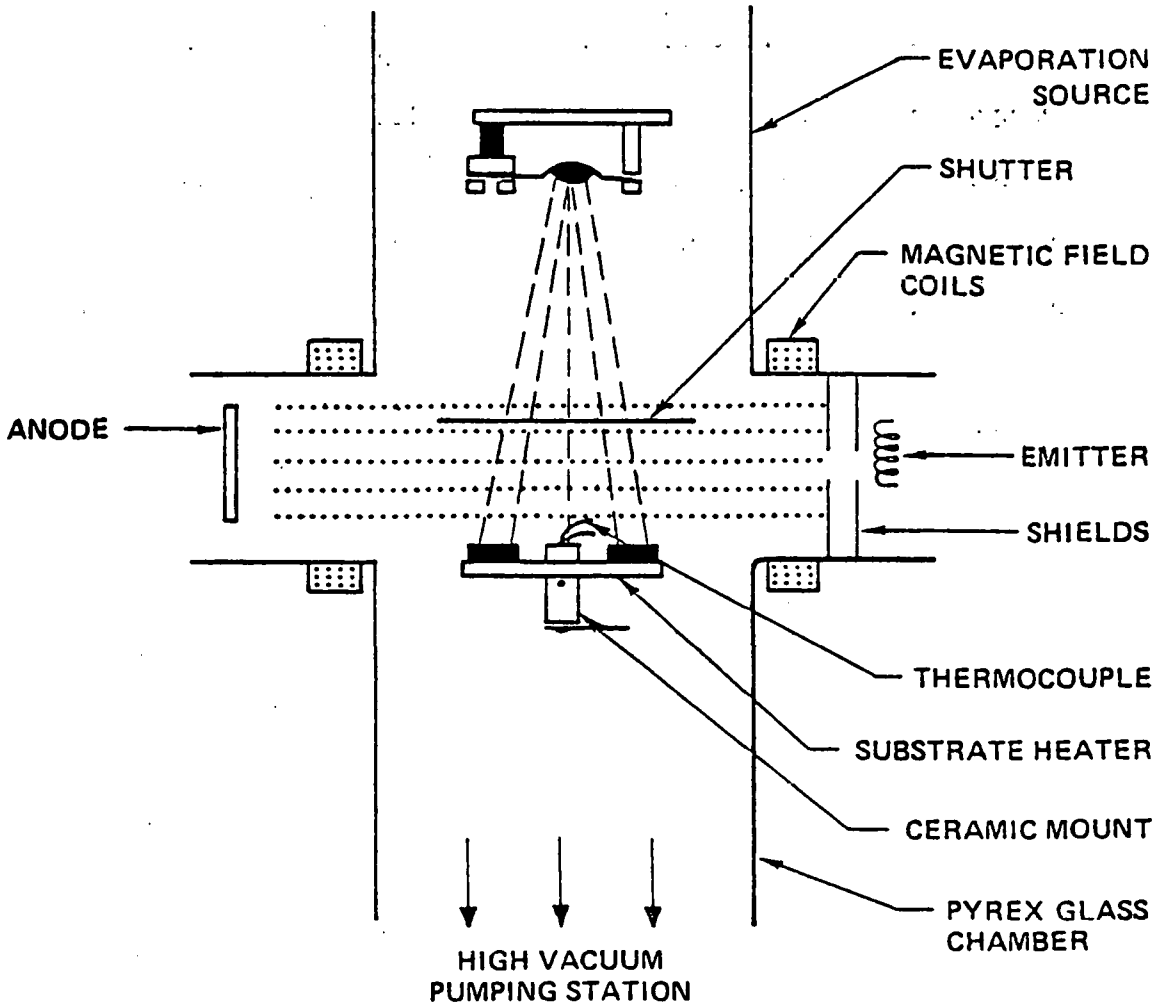

Figure 27. Schematic Diagram of the Experimental Setup for Activated Reactive Deposition of In_2O_3 and $In_2O_3(Sn)$ Films Using Resistance Heated Evaporation Sources. The vapor flux can also be directed upwards.

the system by a calibrated leak valve. The pressure during deposition was maintained at 1×10^{-4} torr. In order to enhance the reactivity of the In/In-Sn vapor species with the reaction gas, a dense plasma was generated by employing a thoriated tungsten emitter and a low voltage anode assembly. Magnetic field coils were used to confine the plasma and further enhance the reaction.

The films were prepared by evaporating In (99.999%) and In-Sn(10-20 at .%) in the presence of a gas mixture of Ar + O_2 onto chemically cleaned glass and quartz substrates. The deposition rate was 0.04 μm/min and typical thickness was ~0.4 μm. The substrate temperature was kept at 350°C. The crystallographic structure of the films was analyzed by X-ray diffraction. The optical transmittance was measured as a function of wavelength between 0.3 and 1.8 μm. The sheet resistance and electrical resistivity were measured by a conventional four probe arrangement.

Bulk In_2O_3 crystallizes in cubic Tl_2O_3 bixbyte structure.[33] X-ray diffractometer measurements on pure In_2O_3 and doped In_2O_3(Sn) films revealed a similar structure. X-ray diffractograms for a pure In_2O_3 and In_2O_3(Sn) (18 at .%) films are shown in Fig. 28. In the In_2O_3(Sn) films no SnO_2 phase was detected implying Sn replaces In substitutionally in the bcc lattice. This observation is in accordance with the observation of a large number of workers on these films prepared by different techniques.[34-38] As revealed by the intensity distribution of the X-ray diffraction patterns, whereas pure In_2O_3 films show a preferred orientation in the (100) direction, In_2O_3(Sn) films exhibit a (111) preferred orientation. A (111) orientation in sputtered[35,39] and CVD[37,38] In_2O_3(Sn) films has been reported in the

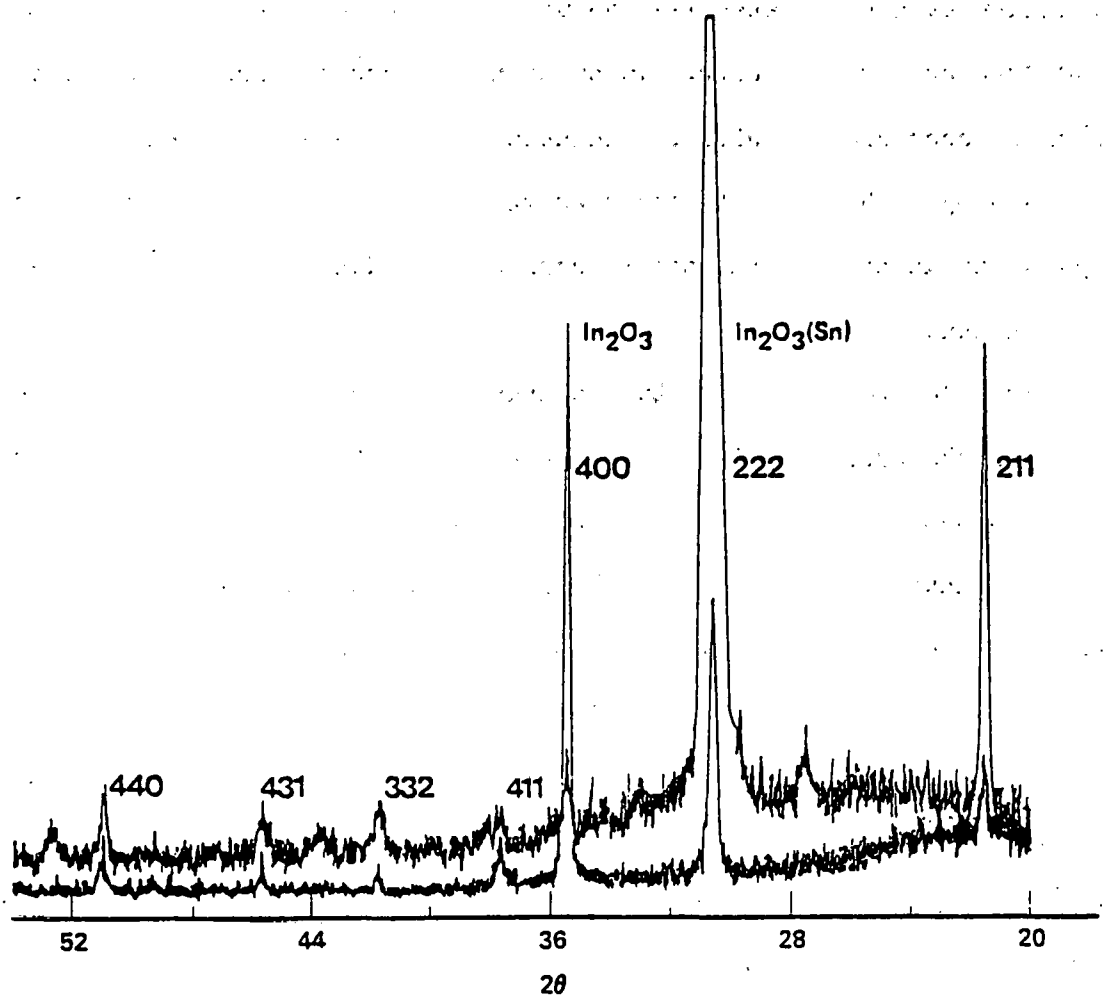

Figure 28. X-ray Diffraction Data for In_2O_3 and In_2O_3(Sn) Films

literature. Vossen[34] has also reported (100) preferred orientation in his sputtered In_2O_3(Sn) films. It may be pointed out that the preferred orientation depends on the deposition conditions.

Figure 29 shows the transmittance as a function of wavelength for In_2O_3 and In_2O_3(Sn) films. It is seen that both In_2O_3 and In_2O_3(Sn) show identical behavior and the transmittance increases rapidly at a wavelength

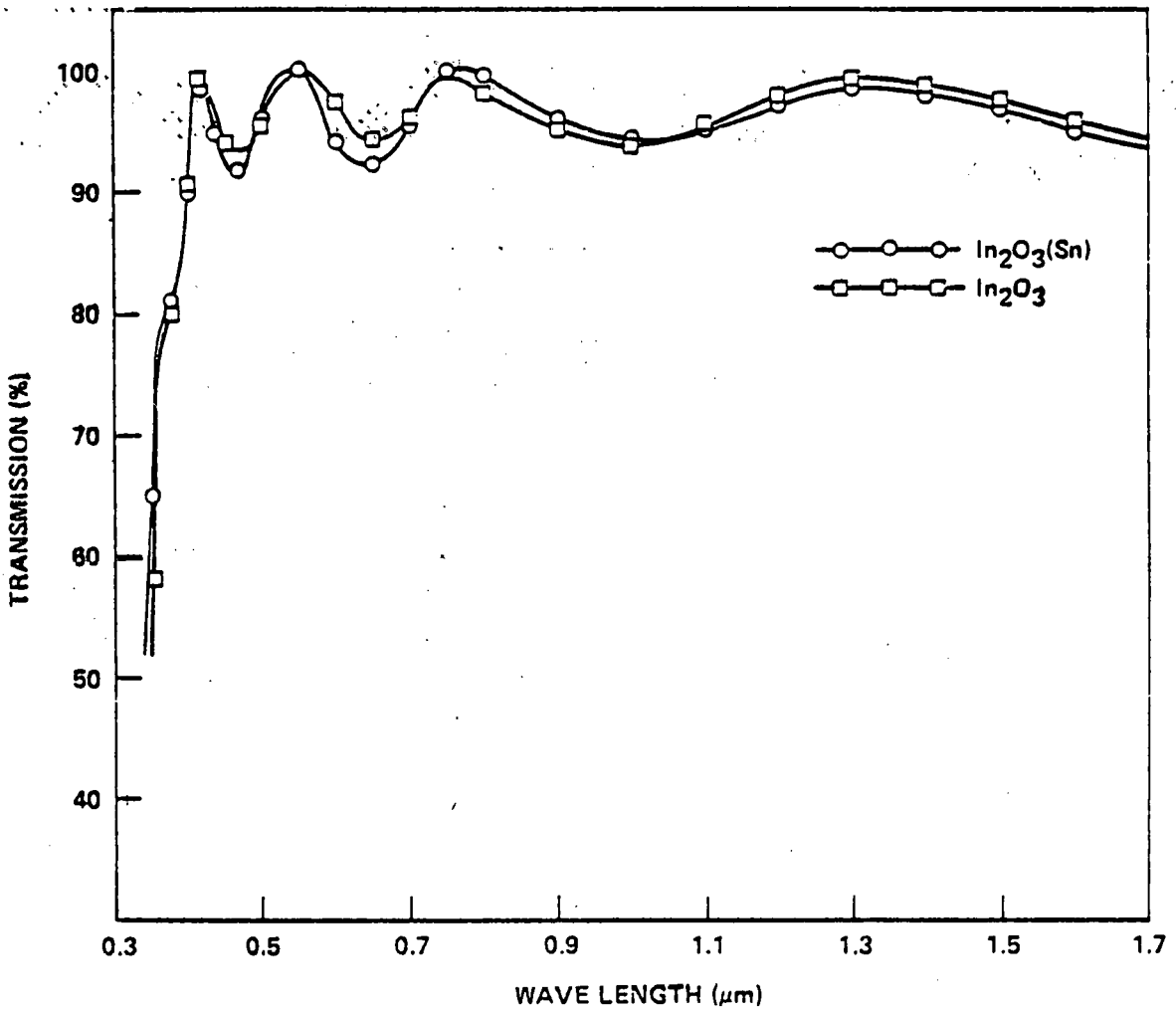

Figure 29. Transmission vs. Wavelength for In_2O_3 (-0-0-) 80 Ω/□ and In_2O_3(Sn) (□-□-) 25 Ω/□ films

of 0.35 μm, thus indicating the absorption edge for these films to be at 0.35 μm (3.54 eV). Table 7 summarizes the electrical and optical properties in In_2O_3 and In_2O_3(Sn) films. It is seen that the films with a sheet resistance of 25 Ω/□ have an average transmittance of 0.96 from 0.4 - 1.8 μm. It may be pointed out that the film thickness is 0.4 μm and by sacrificing few percent on transmittance, films with lower sheet resistance have been made.

TABLE 7

Properties of In_2O_3(Sn) Films Prepared by Activated Reactive Evaporation Technique

Film	Sheet Resistance (ohm/□)	Integrated Transmittance
In_2O_3	80	0.96 (Between 0.6 and 1.6 μm)
In_2O_3(Sn)	25	0.96 (Between 0.6 and 1.6 μm)
In_2O_3(Sn)	2.2	0.88 (0.4 and 1.1 μm)

For example ~1 μm thick films have a sheet resistance of 2.2 Ω/□ and an average transmittance of 0.88 from 0.4 - 1.1 μm. The sheet resistance as a function of Sn concentration in the In-Sn alloy is shown in Figure 30. It is seen that the sheet resistance decreases rapidly with increasing Sn concentration. Also given in the figure is the integrated (over 0.4 - 1.2 μm) value of transmittance for these films. It should be noted that whereas the sheet resistance is a strong function of Sn concentration, the transmittance is only weakly dependent on it.

Electrical resistivity measurements have also been carried out on In_2O_3:Sn (18%) films deposited at temperatures ranging from room temperature to 400°C. The electrical resistivity is found to be strongly dependent on the deposition temperature as shown in Figure 31. The resistivity decreases with increasing deposition temperature. Beyond 250°C the electrical resistivity decreases very rapidly. Transmittance measurements on these films show that films deposited at all temperatures are highly transparent (>90%) over a wavelength region of 0.6 to 1.2 μM.

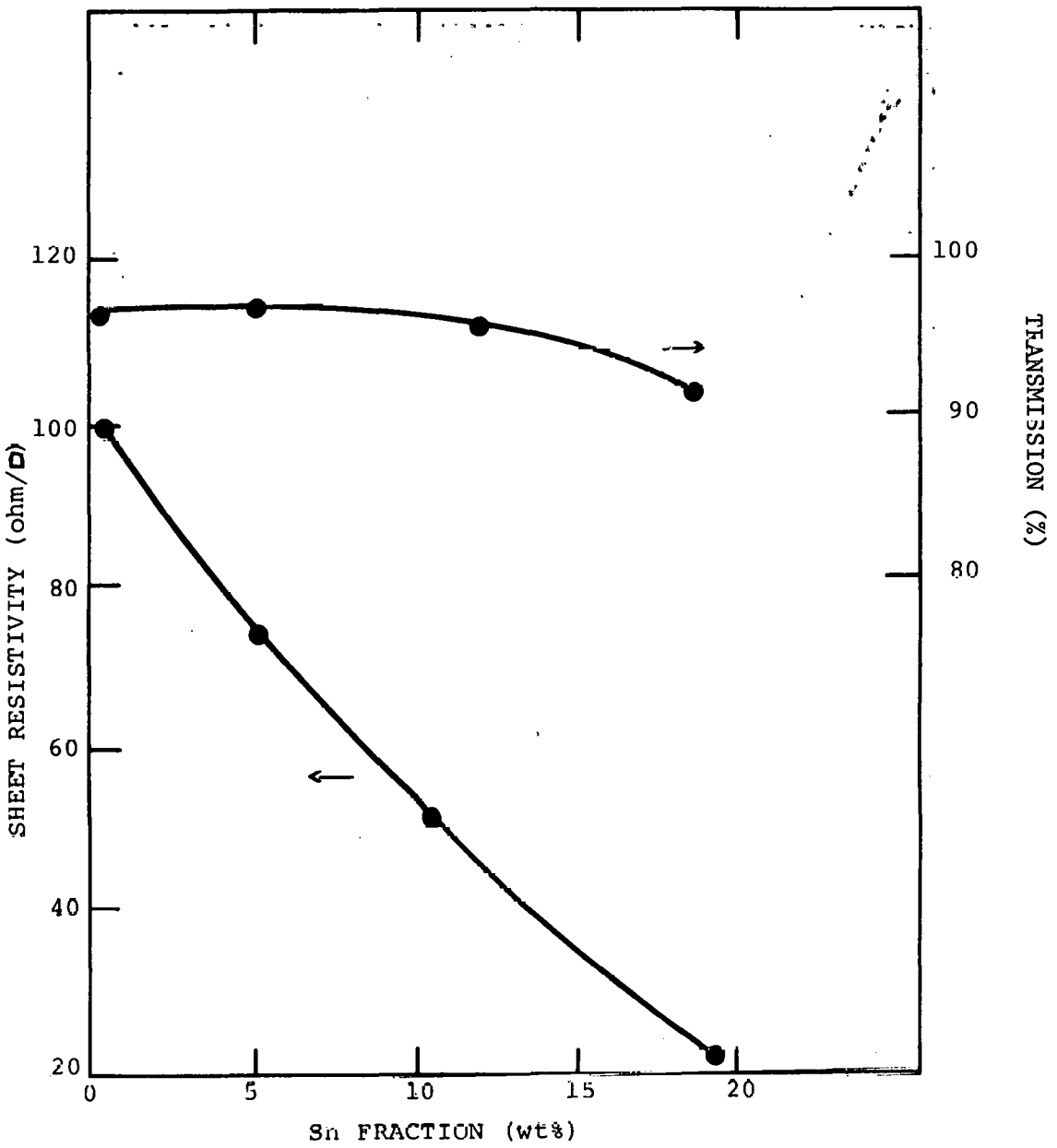

Figure 30. Sheet Resistivity and Transmission vs. Sn Concentration of ITO Films

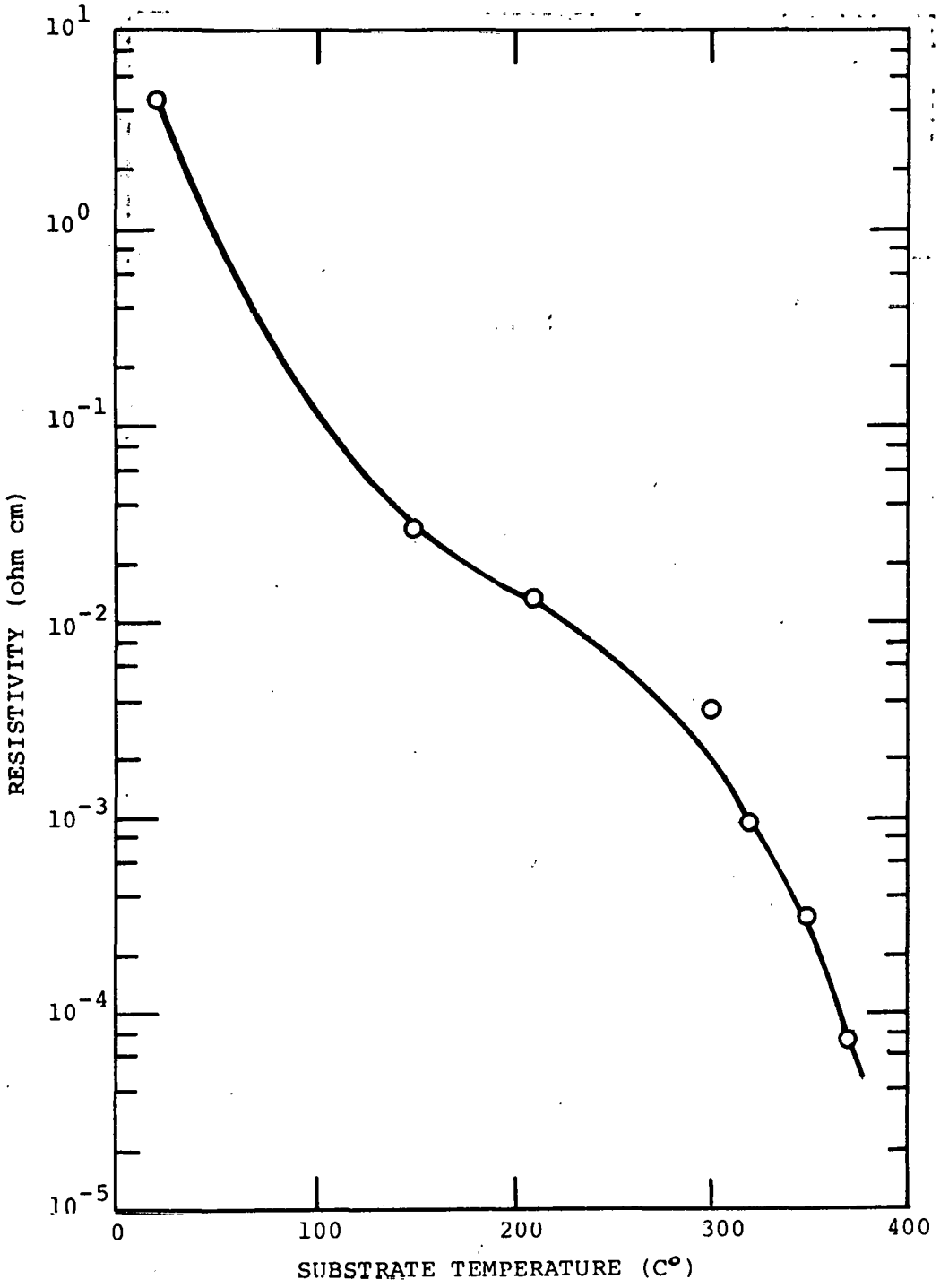

Figure 31. Resistivity vs. Substrate Temperature of ITO Films

It would be useful to compare the performance of the In_2O_3(Sn) films prepared by this Activated Reactive Evaporation technique with the conducting transparent coatings prepared by other techniques. The results for different types of coatings prepared by a variety of techniques such as pyrolysis, CVD, reactive sputtering and sputtering of oxide targets are summarized in Table 8. Also given are the values of "figure of merit"[40] $\left(\frac{T^{10}}{R}\right)$ for the various coatings. It is seen that In_2O_3(Sn) films prepared by our technique clearly demonstrate much better optical characteristics. The films have an optical transparency of 0.99 at certain wavelengths and over 0.95 even up to wavelengths as high as 1.6 μm. Apart from this, whereas, our technique involves no post-deposition treatment, all the films reported by other investigators receive some kind of post-deposition treatment involving temperatures as high as 400-700°C in a variety of ambients.

TABLE 8

Comparison of the Performance of Transparent Conducting Films Prepared by Different Techniques

Material	Technique	R_s ohm/□	Transmittance at Various Wavelengths					Figure of Merit ($T^{10}/R_s \times 10^{-3}$)					Reference
			0.4 μm	0.6 μm	0.8 μm	1.2 μm	1.6 μm	0.4 μm	0.6 μm	0.8 μm	1.2 μm	1.6 μm	
In_2O_3:(Sn)	Activated Reactive Evaporation	2.2	0.79	0.91	0.91	0.80	0.58	43	177	177	54	2	Present Work
In_2O_3:(Sn)	Activated Reactive Evaporation	25	0.91	0.94	0.97	0.97	0.95	17	21.5	29.5	29.5	27	Present Work
In_2O_3:(Sn)	Reactive Sputtering	3	0.70	0.84	0.84	0.50	0.20	9	58	58	0.3	--	41
In_2O_3:(Sn)	Powder Target Sputtering	7	0.80	0.80	0.81	0.53	0.08	15	15	17	0.2	--	39
In_2O_3:(Sn)	Pyrolysis	13.6	0.74	0.86	0.92	0.92	0.72	0.36	16	32	32	0.27	42
SnO_2	Spray	6	0.60	0.78	0.82	0.55	0.20	1	14	23	0.42	--	41
Cd_2SnO_4	Sputtering	1.34	0.10	0.83	0.78	0.38	0.10	--	116	62	--	--	43

VII. REFERENCES

1 Interim Report for First Year of Effort, ERDA Contract No. E(49-18)-2457, Monosolar, Inc., (1977)

2 M.P.R. Panicker, M. Knaster and F.A. Kröger, J. Electrochem. Soc., 125, 566 (1978)

3 F.A. Kröger, J. Electrochem. Soc., 125, 2028 (1978)

4 N.V. Agrinskaya, E.N. Arkadeva, O.A. Matveev and Yu.V. Rud, Sov. Phys. Semicond., 2, 776 (1969)

5 V.A. Chapnin, Sov. Phys. Semicond., 3, 481 (1969)

6 A.P. Didkovskii and V.I. Khivrich, Phys. Stat. Sol. (a), 32, 621 (1975)

7 E.N. Arkadeva and O.A. Matveev, Rev. Phys. Appl., 12, 239 (1977)

8 F.A. Kröger and K. Lehovec, "Development of Large Area Solar Cells Based on CdTe", University of Southern California Final Report, under Monosolar DOE Contract No. EX-76-C-01-2457, (1978)

9 See for example, R.H. Bube, "Photoconductivity of Solids", John Wiley & Sons, Inc., New York (1960)

10 M.R. Lorenz, B. Segall and H.H. Woodbury, Phys. Rev., 134, A751 (1964)

11 C.W. Isoler, J.A. Kafalas, A.J. Strauss, H.F. Macmillan and R.H. Bube, Solid State Commun., 10, 619 (1972)

12 D.L. Losee, R.P. Khosla, D.K. Ranadive and F.T.J. Smith, Solid State Commun., 13, 819 (1973)

13 A. Rose, "Concepts in Photoconductivity and Allied Problems", ed. by R.E. Marshak, Interscience Publishers, a division of John Wiley & Sons, New York (1963)

14 M.A. Lampert and P. Mark, "Current Injection in Solids", Academic Press, New York (1970)

15 C. Scharager, J.C. Muller, R. Stuck and P. Siffert, Phys. Stat. Sol. (a), 31, 247 (1975)

16 Y. Marfaing, J. Lascaray and R. Triboulet, Metal Semiconductor Contacts Conf. ser. 22, p. 201, Inst. Phys., London (1974)

17 B. Rabin, H. Tabatabai and P. Siffert, Phys. Stat. Sol. (a), 49, 577 (1978)

18 C. Canali, M.A. Nicolet and J.W. Mayer, Solid State Electron, 18, 871 (1975)

19 A.M. Mancini, C. Manfredotti, C. De Blasi, G. Micocci and A. Tepore, Rev. Phys. Appl., 12, 255 (1977)

20 K.P. Pande and G.G. Roberts, IEEE Trans. Nucl. Sci., 24, 2017 (1977)

21 C. Lhermitte, C. Vautier, Thin Solid Films, 58, 83 (1979)

22 See for example, E.H. Rhoderick, "Metal Semiconductor Contacts", Clarendon Press, (1978)

23 G.H. Parker and C.A. Mead, Phys. Rev., 184, 780 (1969)

24 J.P. Ponpon and P. Siffert, Rev. Phys. Appl., 12, 427 (1977)

25 A.J. Dabrowski, J. Chwaszczewska, J. Iwanczyk, R. Triboulet and Y. Marfaing, Rev. Phys. Appl., 12, 296 (1977)

26 A. Cornet, P. Siffert, A. Coche and R. Triboulet, Appl. Phys. Letters, 17, 432 (1970)

27 J.W. Mayer, J. Appl. Phys., 38, 296 (1967)

28 P.G. Kasherninov, O.A. Matveev and L.M. Maslova, Sov. Phys. Semicond., 3, 451 (1969)

29 E. Schibli and A.G. Milnes, Solid State Electron., 11, 323 (1968)

30 C.T. Sah, R.N. Noyce and W. Shockley, Proc. IRE 45, 1228 (1957)

31 J.L. Vossen, Physics of Thin Films, Eds. G. Hass, M.P. Francombe and R.W. Hoffman, Vol. 9, 1 (1977) Academic Press N.Y.

32 G. Haacke, Ann. Rev. Mater. Sci. 7, 73 (1977)

33 R.W.C. Wyckoff, "Crystal Structures", 2nd Ed., Vol. 1-3, Wiley, Interscience N.Y. (1963)

34 J.L. Vossen, RCA Rev. 32, 289 (1971)

35 M. Hecq, A. Dubois and J. Van Cakenberghe, Thin Solid Films, 10, 117 (1973)

36 J.R. Bosnell and R. Waghorne, Thin Solid Films, 15, 161 (1973)

37 H. Köston, R. Jost and W. Lens, Phys. Stat. Sol. 29a, 87 (1975)

38 J.C. Manifacier, L. Szepessy, J.F. Bresse, M. Perotin and R. Stuke, Mat. Res. Bull. 14, 109 (1979)

39 D.B. Fraser and H.D. Cook, J. Electrochemical Soc., 119, 13688 (1972)

40 G. Haacke, J. Appl. Phys. 47, 4086 (1976)

41 D.M. Mattox, J. Vac. Sci. Tech., 12, 5, 1023 (1975)

42 J.C. Manifaciar, L. Szepessy, J.E. Bresse, M. Perotin and R. Stuke, Mat. Res. Bull. 16, 163 (1979)

43 G. Haacke, W.E. Mealmaker and L.A. Siegel, Thin Solid Films, 55, 67 (1978)

☆U.S. GOVERNMENT PRINTING OFFICE: 1980-740-145/676